

Singular Value and Frame Decomposition-based Reconstruction for Atmospheric Tomography

Lukas Weissinger* Simon Hubmer* Bernadett Stadler*
 Ronny Ramlau*[†]

July 10, 2024

Abstract

Atmospheric tomography, the problem of reconstructing atmospheric turbulence profiles from wavefront sensor measurements, is an integral part of many adaptive optics systems used for enhancing the image quality of ground-based telescopes. Singular-value and frame decompositions of the underlying atmospheric tomography operator can reveal useful analytical information on this inverse problem, as well as serve as the basis of efficient numerical reconstruction algorithms. In this paper, we extend existing singular value decompositions to more realistic Sobolev settings including weighted inner products, and derive an explicit representation of a frame-based (approximate) solution operator. These investigations form the basis of efficient numerical solution methods, which we analyze via numerical simulations for the challenging, real-world Adaptive Optics system of the Extremely Large Telescope using the entirely MATLAB-based simulation tool MOST.

Keywords. Atmospheric Tomography, Singular Value Decomposition, Frame Decomposition, Adaptive Optics, Inverse and Ill-Posed Problems

1 Introduction

Adaptive Optics (AO) is an essential component of ground-based telescopes such as the Extremely Large Telescope (ELT) [17] of the European Southern Observatory (ESO), currently under construction in the Atacama desert in Chile. This is because temperature fluctuations in the atmosphere cause turbulence, which results in wavefront aberrations of the incoming light before it reaches the telescope. If not

*Johann Radon Institute Linz, Altenbergerstraße 69, A-4040 Linz, Austria, (lukas.weissinger@ricam.oeaw.ac.at, simon.hubmer@ricam.oeaw.ac.at, bernadett.stadler@indmath.uni-linz.ac.at, ronny.ramlau@ricam.oeaw.ac.at).

[†]Johannes Kepler University Linz, Institute of Industrial Mathematics, Altenbergerstraße 69, A-4040 Linz, Austria, (ronny.ramlau@jku.at).

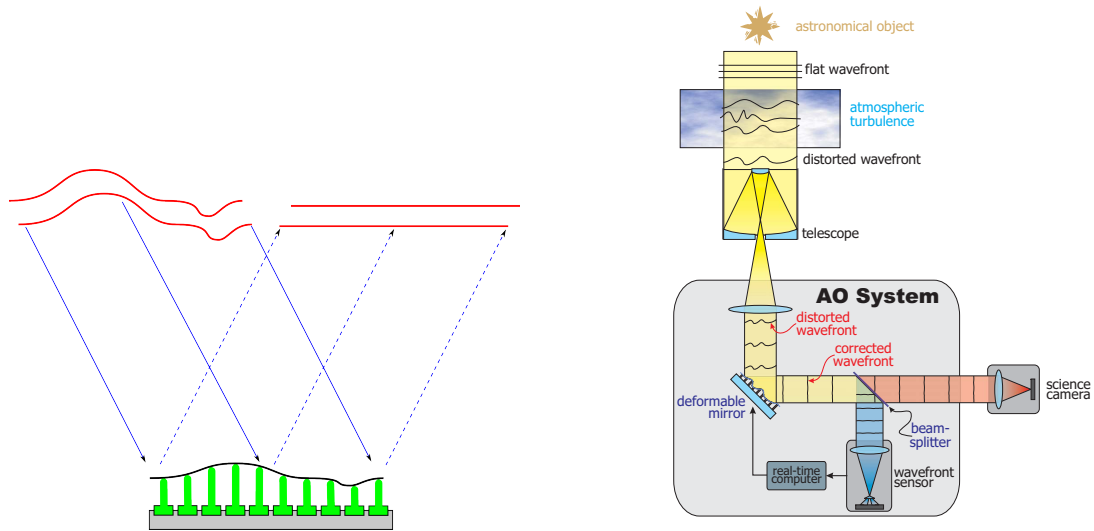


Figure 1.1: Schematic depiction of wavefront correction via deformable mirror (left, image from [2]) and working principle of a SCAO system (right, image from [10]).

corrected by an AO system, these aberrations result in blurred images and therefore a severe loss of image quality. The general working principle of an AO system can be summarized as follows [44, 45, 11]: First, a wavefront sensor (WFS) is used to measure the wavefront aberration of the incoming light of some reference light source such as a natural guide stars (NGS). Then, a deformable mirror (DM) located in the light path is adjusted, such that after reflection from this DM, the incoming wavefront is approximately plane and thus aberration free; see Figure 1.1 (left). Since the atmosphere is rapidly changing, this measurement and correction cycle has to be repeated continuously at a frequency of about 500 Hz.

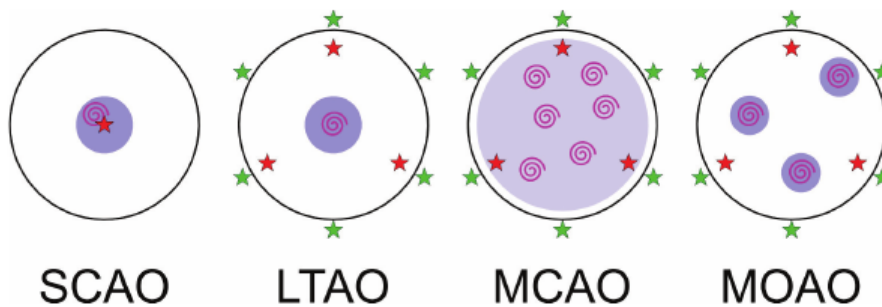


Figure 1.2: Schematic depiction of different types of AO systems. Magenta spirals represent astronomical objects of interest, while red and greens stars correspond to locations of NGS and LGS, respectively. The darker shaded areas correspond to the directions corrected for by the corresponding AO systems. Image taken from [2].

The AO correction procedure outlined above forms the basis of so-called Single

Conjugate Adaptive Optics (SCAO), which is used to observe astronomical objects in the near vicinity of a bright reference star; see Figure 1.1 (left) for a schematic depiction. However, if the distance between the object of interest and this NGS is too large, the image quality strongly deteriorates. This is due to the directional dependence of the wavefront aberration, caused by different atmospheric turbulence. Therefore, the WFS measurement in guide star direction is then no longer close to that of the observed object. A common remedy for this problem is to consider multiple guide stars, both NGS and artificial laser guide stars (LGS) created by powerful lasers in the sodium layer of the atmosphere. The incoming wavefront of each of those guide stars is measured by a separate WFS, from which one then aims to reconstruct the entire turbulence volume above the telescope. This is the atmospheric tomography problem considered in this paper. Once the atmospheric turbulence has been reconstructed, it is then possible to use one or several DMs to correct for objects with no guide star nearby, or obtain a correction over either a larger field of view (FoV) or in several view directions. These settings correspond to Laser Tomography Adaptive Optics (LTAO), Multiconjugate Adaptive Optics (MCAO), and Multiobject Adaptive Optics (MOAO), respectively, which are illustrated in Figure 1.2. For further details see e.g. [8, 1, 26, 36, 43].

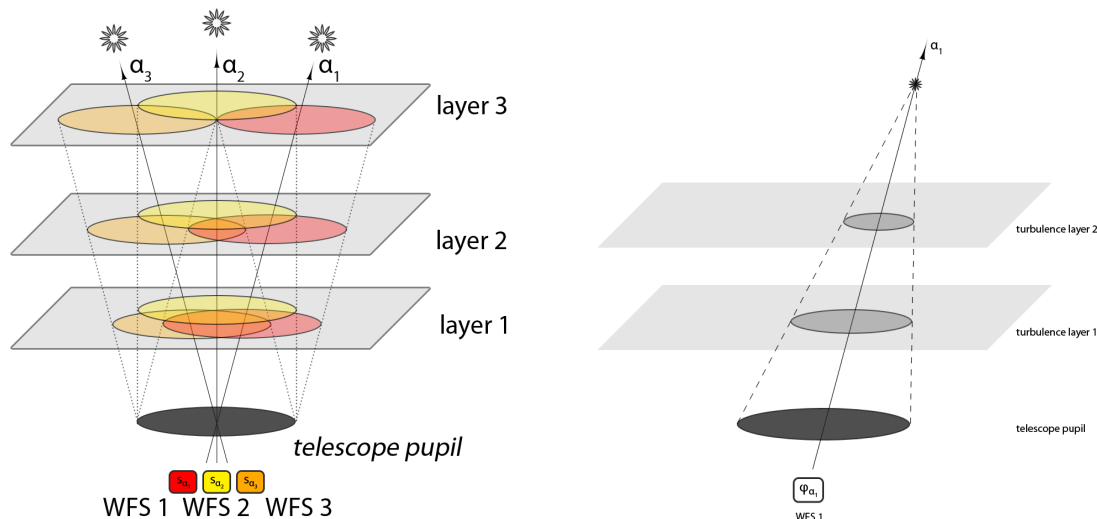


Figure 1.3: Illustration of the atmospheric tomography problem with three turbulence layers, NGSs and corresponding WFSs (left). Light stemming from a single LGS is influenced by the cone effect (right). Images taken from [58].

In the form introduced above, atmospheric tomography falls into the category of limited-angle tomography problems: only a small number of guide stars is available (6 LGS for the ELT), and the NGS and LGS only have a small angle of separation (1 arcmin for MCAO and 3.5 arcmin for MOAO). As such, it is severely ill-posed and thus practically infeasible without additional restrictions [6, 33]. These come in the form of assumptions on the structure of the atmosphere, more precisely that it consists of a finite number of (infinitely) thin turbulent layers located at predefined

heights. Atmospheric tomography then reduces to reconstructing the atmospheric turbulence profile on those finitely many layers from the given WFS measurements. An example of this problem for the case of three layers and three (natural) guide stars with corresponding WFSs is depicted in Figure 1.3 (left).

The atmospheric tomography problem has attracted considerable attention in the past. Among the many proposed reconstruction methods we mention e.g. the minimum mean square error method [19], the back-projection algorithm of [20], conjugate gradient type iterative reconstruction methods with suitable preconditioning [13, 25, 22, 57, 55], the Fractal Iterative Method (FrIM) [52, 53, 54], the Finite Element Wavelet Hybrid Algorithm (FEWHA) [58, 59, 60, 50, 49], as well as a Kaczmarz iteration [39, 46]. For further methods as well as important practical considerations see also [12, 24, 23, 35, 37, 38, 48] and the references therein. In recent years FEWHA has already proven in simulations to provide an excellent reconstruction quality in real-time for the MORFEO instrument of the ELT [51]. A clever discretization strategy together with a matrix-free implementation and a small number of conjugate gradient iterations makes reconstructions in real-time possible and enables on the fly parameter updates.

While these methods have all been studied in detail both analytically and numerically, they do not yield much new knowledge about the atmospheric tomography problem itself. This should be contrasted with the (limited-angle) tomography operator, from which the atmospheric tomography operator is derived [11, 19]. There, a large number of theoretical results offer insight into the structure and ill-posedness of the classic tomography problem [33]. Many of these are directly related to the availability of a singular value decomposition (SVD) of the (limited-angle) Radon transform [6, 33]. Motivated by this, a singular value-type decomposition (SVTD) of the atmospheric tomography operator has recently been derived in [34], and has provided the first theoretical insights into the ill-posedness of the atmospheric tomography problem. However, this SVTD is only valid on a square telescope aperture in a NGS-only setting, which limits its practical applicability. This motivated the derivation of a frame decomposition (FD) in [27], which provided an SVD-like decomposition of the atmospheric tomography operator valid for general aperture shapes and a mixture of both NGS and LGS. The main drawback of this approach is that it only provides an approximate solution to the problem; see also [56]. Note that in [27] an SVTD was also derived for square apertures and a LGS-only setting. Further analytic properties including the non-uniqueness of the atmospheric tomography problem have recently been considered in [42].

In this paper, we aim to advance the study of the atmospheric tomography problem in two ways: First, we extend the previously derived SVTDs in the NGS-only and LGS-only cases to a more physically realistic setting. In particular, we consider real-order Sobolev spaces for the definition space of the operator, which is motivated by the Kolmogorov turbulence model for the atmospheric layers [30]. Furthermore, we incorporate commonly used turbulence profiles into the SVTDs by replacing the standard inner products with correspondingly weighted version. Furthermore, we consider a split-tomography approach to solve the atmospheric tomography prob-

lem in the mixed NGS/LGS problem using the derived SVTDs. Secondly, for the FD of the atmospheric tomography operator, we derive an explicit representation of the involved dual frame functions, which previously had to be computed numerically. This in turn leads to an explicit representation of the (approximate) frame inverse, which allows for a highly efficient implementation. The final contribution of this paper is a numerical comparison of the SVTDs and FD with state-of-the-art reconstruction algorithms in a realistic adaptive optics simulation environment.

The outline of this paper is as follows: In Section 2, we recall the definition and some basic properties of the atmospheric tomography operator. In Section 3, we then derive a singular value decomposition of this operator in a realistic Sobolev space setting including general weighted inner products incorporating turbulence profiles. In Section 4, we then consider a frame decomposition of the atmospheric tomography operator, and derive an explicit representation of the involved dual frame functions and the corresponding (approximate) solution operator. Finally, in Section 4, we numerically test the resulting reconstruction methods in a realistic environment using the adaptive optics simulation tool MOST, and compare the results to those obtained with two other state-of-the-art reconstruction algorithms.

2 The Atmospheric Tomography Operator

In this section, we recall the definition and some basic properties of the atmospheric tomography operator, which has originally been derived from the (limited-angle) Radon transform using the layered structure of the atmospheric turbulence [11, 19].

First, let the domain $\Omega_A \subset \mathbb{R}^2$ represent the telescope aperture, which typically (but not always) is a circular and symmetric domain centered around the origin. Furthermore, assume that there are L atmospheric layers, i.e., planes parallel to the aperture Ω_A , located at distinct heights $h_\ell \in \mathbb{R}_0^+$ for $\ell = 1, \dots, L$. We assume that the heights are given in ascending order and note that typically $h_1 = 0$. Note that all 2-dimensional domains defined here are embedded in \mathbb{R}^3 by fixing the z-coordinate. Next, consider G different guide stars with corresponding direction vectors $\alpha_g = (\alpha_g^x, \alpha_g^y) \in \mathbb{R}^2$ for $g = 1, \dots, G$. The vectors α_g are such that seen from the center of the telescope aperture, the vectors $(\alpha_g^x, \alpha_g^y, 1) \in \mathbb{R}^3$ point directly at the corresponding guide stars. Now, assume that the first G_{NGS} guide stars are NGS, while the remaining G_{LGS} guide stars are LGS, such that $G = G_{\text{NGS}} + G_{\text{LGS}}$. Then we can define the coefficients

$$c_{\ell,g} = \begin{cases} 1, & g \in \{1, \dots, G_{\text{NGS}}\}, \\ 1 - h_\ell/h_{\text{LGS}}, & g \in \{G_{\text{NGS}} + 1, \dots, G\}, \end{cases}$$

where h_{LGS} denotes the height of the sodium layer in the atmosphere in which LGS are created (approximately 90 km). The coefficients $c_{\ell,g}$ model the cone effect for LGS as illustrated in Figure 1.3 (right). Note that since $h_\ell < h_{\text{LGS}}$ for all

$\ell = 1, \dots, L$, we have $c_{\ell,g} \in (0, 1]$. Next, we introduce the domains

$$\Omega_\ell := \bigcup_{g=1}^G \Omega_A(\alpha_g h_\ell) \subset \mathbb{R}^2, \quad \forall \ell = 1, \dots, L,$$

where

$$\Omega_A(\alpha_g h_\ell) := \left\{ r \in \mathbb{R}^2 \mid \frac{r - \alpha_g h_\ell}{c_{\ell,g}} \in \Omega_A \right\}.$$

The domains Ω_ℓ are exactly those parts of the atmospheric layers which are “seen” by the WFSs. Consequently, these are also the only parts of the atmosphere which one can hope to reconstruct accurately. In the example shown in Figure 1.3 (left), the domains Ω_ℓ correspond to the union of the coloured areas; see also Figure 2.1.

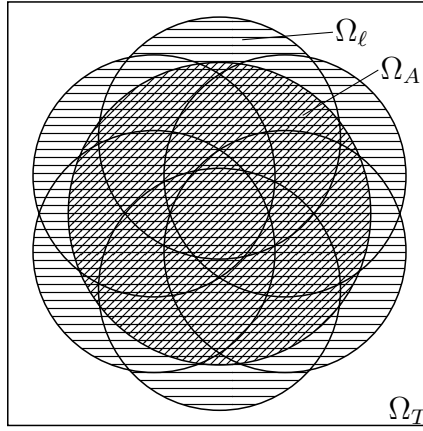


Figure 2.1: A schematic drawing of the domains Ω_A , Ω_ℓ , and Ω_T .

We now want to define the atmospheric tomography operator between suitable Lebesgue spaces. For this, we introduce the space $L_2(\Omega, \gamma)$ with $\gamma > 0$, by which we simply mean the classic Lebesgue space $L_2(\Omega)$ equipped with the scaled inner product

$$\langle u, v \rangle_{L_2(\Omega, \gamma)} := \frac{1}{\gamma} \int_{\Omega} u(r) \overline{v(r)} dr.$$

Let $\phi = (\phi_\ell)_{\ell=1, \dots, L}$ denote the refractive index variations (a dimensionless quantity), related to temperature fluctuations within the atmosphere, causing atmospheric turbulence, and let $\varphi = (\varphi_g)_{g=1, \dots, G}$ denote the incoming wavefronts as reconstructed by the WFSs. Then for given turbulence weights $(\gamma_\ell)_{\ell=1, \dots, L}$ the atmospheric tomography operator can be defined as [19]

$$A : \mathcal{D}(A) := \prod_{\ell=1}^L L_2(\Omega_\ell, \gamma_\ell) \rightarrow L_2(\Omega_A)^G, \quad \phi = (\phi_\ell)_{\ell=1}^L \mapsto \varphi = ((A_g \phi))_{g=1}^G, \quad (2.1)$$

$$(A_g \phi)(r) := \sum_{\ell=1}^L \phi_\ell (c_{\ell,g} r + \alpha_g h_\ell).$$

Note that the product spaces above are equipped with the canonical inner products

$$\langle \phi, \psi \rangle_{\prod_{\ell=1}^L L_2(\Omega_\ell, \gamma_\ell)} = \sum_{\ell=1}^L \langle \phi_\ell, \psi_\ell \rangle_{L_2(\Omega_\ell, \gamma_\ell)} = \sum_{\ell=1}^L \frac{1}{\gamma_\ell} \langle \phi_\ell, \psi_\ell \rangle_{L_2(\Omega_\ell)},$$

and

$$\langle \varphi, \theta \rangle_{L_2(\Omega_A)^G} = \sum_{g=1}^G \langle \varphi_g, \theta_g \rangle_{L_2(\Omega_A)}.$$

The atmospheric tomography operator A as defined in (2.1) essentially only sums up the contributions of each turbulence layer in the direction of the guide stars. The weights γ_ℓ are used to place a higher emphasis on layers on which a strong turbulence is expected, and are assumed to satisfy $\sum_{\ell=1}^L \gamma_\ell = 1$. In practice, they are known quantities derived from previously measured turbulence profiles. Note that from a mathematical point of view, one may also consider non-constant (i.e. spatially varying) weights γ_ℓ , thereby placing a varying emphasis on certain areas within the atmospheric layers. An example are the piecewise constant weights introduced in [48], which are also briefly discussed at the end of Section 4. Since they are not commonly used in practice, we do not consider such spatially varying weights here, but note that our subsequent analysis could be extended to include them as well.

For further use, we also require the adjoint of the atmospheric tomography operator A , which following [39, Proposition 2] can be derived to be

$$(A^* \varphi)(r) = \sum_{g=1}^G (A_g^* \varphi)(r) = \sum_{g=1}^G \left(\frac{\gamma_\ell}{c_{\ell,g}^2} \varphi_g \left(\frac{r - \alpha_g h_\ell}{c_{\ell,g}} \right) I_{\Omega_A(\alpha_g h_\ell)}(r) \right)_{l=1}^L, \quad (2.2)$$

where $I_{\Omega_A(\alpha_g h_\ell)}$ denotes the indicator function of the domain $\Omega_A(\alpha_g h_\ell)$. It was shown in [34] that the atmospheric tomography operator A is not compact, and thus an SVD does not necessarily need to exist. Nevertheless, an SVTD can be derived for a “periodic” atmospheric tomography operator on a square domain, which we now introduce in a general Sobolev setting. For this, let $\Omega_T = [-T, T]^2 \subset \mathbb{R}^2$ be a square domain with T chosen sufficiently large such that, cf. Figure 2.1,

$$\Omega_A + \alpha_g h_\ell \subset c_\ell \Omega_T, \quad \forall g = 1, \dots, G, \quad \forall \ell = 1, \dots, L, \quad (2.3)$$

where

$$c_\ell := \min_{g=1, \dots, G} \{c_{\ell,g}\}, \quad \forall \ell = 1, \dots, L.$$

Then, we introduce the *periodic* Sobolev spaces $H^s(c_\ell \Omega_T, \gamma_\ell)$ via the inner product

$$\langle u, v \rangle_{H^s(c_\ell \Omega_T, \gamma_\ell)} := \sum_{j,k \in \mathbb{Z}} (1 + \beta_{\ell,T} |(j,k)|^2)^s u_{jk,\ell} \overline{v_{jk,\ell}}, \quad \beta_{\ell,T} = \pi^2 (c_\ell T)^{-2}, \quad (2.4)$$

where $u_{jk,\ell} := \langle u, w_{jk,\ell} \rangle_{L_2(c_\ell \Omega_T, \gamma_\ell)}$ and $v_{jk,\ell} := \langle v, w_{jk,\ell} \rangle_{L_2(c_\ell \Omega_T, \gamma_\ell)}$ with

$$w_{jk,\ell}(x, y) := \frac{\gamma_\ell^{1/2}}{c_\ell} w_{jk}((x, y)/c_\ell), \quad \text{and} \quad w_{jk}(x, y) := \frac{1}{2T} e^{i\omega(jx+ky)}, \quad \omega = \frac{\pi}{T}. \quad (2.5)$$

The functions w_{jk} and $w_{jk,\ell}$ defined in (2.5) form orthonormal bases over the spaces $L_2(\Omega_T)$ and $L_2(c_\ell\Omega_T, \gamma_\ell)$, respectively. Note that our definition of $H^s(c_\ell\Omega_T, \gamma_\ell)$ amounts to the classic Fourier-series definition of periodic Sobolev spaces (see e.g. [29, 40]), adapted to our specific scaled domains $c_\ell\Omega_T$ and incorporating the turbulence weights γ_ℓ . For integer order $s \in \mathbb{N}$, the inner product (2.4) is equivalent to the classic Sobolev space inner product [29, Proposition 7.2], while for general $s \in \mathbb{R}$ equivalence holds over the Triebel spaces, which include zero boundary conditions [33]. With this, the periodic atmospheric tomography operator is now defined as

$$\begin{aligned} \tilde{A}^{(s)} : \prod_{\ell=1}^L H^s(c_\ell\Omega_T, \gamma_\ell) &\rightarrow L_2(\Omega_T)^G, & \phi = (\phi_\ell)_{\ell=1}^L &\mapsto \varphi = \left((\tilde{A}_g^{(s)}\phi) \right)_{g=1}^G \\ (\tilde{A}_g^{(s)}\phi)(r) &:= \sum_{\ell=1}^L \phi_\ell(c_{\ell,g}r + \alpha_g h_\ell), \end{aligned}$$

with $0 \leq s \in \mathbb{R}$. The compactness of this operator now depends on the specific choice of s . If $s = 0$, then as above it can be shown that $\tilde{A}^{(0)}$ is not compact, and thus an SVD does not necessarily need to exist. However, if $s > 0$, then the compactness of the Sobolev embedding operator on the bounded domain Ω_T implies that $\tilde{A}^{(s)}$ is compact, and thus an SVD exists [14]. In the specific case of $s = 0$ and $\gamma_\ell = 1$ for all $\ell = 1, \dots, L$, SVTDs for the NGS-only and LGS-only case have been derived in [34] and [27], respectively. As we shall see below, these leverage algebraic properties of the scaled exponential functions w_{jk} . In particular, it was shown in [34, Theorem 5.1] that if

$$\frac{\alpha_g^x h_\ell}{T} \in \mathbb{Q}, \quad \text{and} \quad \frac{\alpha_g^x h_\ell}{T} \in \mathbb{Q}, \quad \forall g = 1, \dots, G, \quad \forall \ell = 1, \dots, L, \quad (2.6)$$

then the pseudo-inverse $(\tilde{A}^{(0)})^\dagger$ is bounded. Hence, in this setting the (periodic) atmospheric tomography problem is well-posed. Furthermore, one can find examples violating (2.6) which lead to unboundedness of $(\tilde{A}^{(0)})^\dagger$. On the other hand, for $s > 0$ the compactness of $\tilde{A}^{(s)}$ implies that $(\tilde{A}^{(s)})^\dagger$ is always unbounded, and thus the (periodic) atmospheric tomography problem is always ill-posed in this case.

3 Singular Value Type Decompositions

In this section, we derive an SVTD for the periodic atmospheric tomography operator $\tilde{A}^{(s)}$ for the case of either NGS-only or LGS-only. In this case, $c_{\ell,g} = c_\ell$ and thus

$$\begin{aligned} \tilde{A}^{(s)} : \mathcal{D}(\tilde{A}^{(s)}) &:= \prod_{\ell=1}^L H^s(c_\ell\Omega_T, \gamma_\ell) \rightarrow L_2(\Omega_T)^G, & \phi = (\phi_\ell)_{\ell=1}^L &\mapsto \varphi = \left((\tilde{A}_g^{(s)}\phi) \right)_{g=1}^G, \\ (\tilde{A}_g^{(s)}\phi)(r) &= \sum_{\ell=1}^L \phi_\ell(c_\ell r + \alpha_g h_\ell). \end{aligned} \quad (3.1)$$

The upcoming analysis closely follows ideas from [34, 27], and is based on the fact that the functions w_{jk} and $w_{jk,\ell}$ defined in (2.5) form orthonormal bases over the spaces $L_2(\Omega_T)$ and $L_2(c_\ell\Omega_T, \gamma_\ell)$, respectively. This implies the following result.

Lemma 3.1. *Let $s \geq 0$ and $\ell \in \{1, \dots, L\}$ be arbitrary but fixed. Then the functions*

$$w_{jk,\ell}^{(s)} := (1 + \beta_{\ell,T}|(j, k)|^2)^{-s/2} w_{jk,\ell}, \quad (3.2)$$

with $w_{jk,\ell}$ as in (2.5) form an orthonormal basis for the Sobolev-space $H^s(c_\ell\Omega_T, \gamma_\ell)$.

Proof. Let $s \geq 0$ and $\ell \in \{1, \dots, L\}$ be arbitrary but fixed. Since the functions $w_{jk,\ell}$ form an orthonormal basis of $L_2(c_\ell\Omega_T, \gamma_\ell)$, it follows with (2.4) that

$$\begin{aligned} & \left\langle w_{j'k',\ell}^{(s)}, w_{j''k'',\ell}^{(s)} \right\rangle_{H^s(c_\ell\Omega_T, \gamma_\ell)} \\ & \stackrel{(2.4)}{=} \sum_{j,k \in \mathbb{Z}} \left(1 + \frac{\pi^2 |(j, k)|^2}{(c_\ell T)^2} \right)^s \left\langle w_{j'k',\ell}^{(s)}, w_{jk,\ell} \right\rangle_{L_2(c_\ell\Omega_T, \gamma_\ell)} \overline{\left\langle w_{j''k'',\ell}^{(s)}, w_{jk,\ell} \right\rangle_{L_2(c_\ell\Omega_T, \gamma_\ell)}} \\ & \stackrel{(3.2)}{=} \sum_{j,k \in \mathbb{Z}} \left\langle w_{j'k',\ell}, w_{jk,\ell} \right\rangle_{L_2(c_\ell\Omega_T, \gamma_\ell)} \overline{\left\langle w_{j''k'',\ell}, w_{jk,\ell} \right\rangle_{L_2(c_\ell\Omega_T, \gamma_\ell)}} = \delta_{j',j''} \delta_{k',k''}, \end{aligned}$$

and thus the functions $w_{jk,\ell}^{(s)}$ are orthonormal in $H^s(c_\ell\Omega_T, \gamma_\ell)$. In order to show that they are also a basis, note that $H^s(c_\ell\Omega_T, \gamma_\ell) \subset L_2(c_\ell\Omega_T, \gamma_\ell)$, and thus for each $u \in H^s(c_\ell\Omega_T, \gamma_\ell)$ there holds

$$\begin{aligned} u &= \sum_{j,k \in \mathbb{Z}} \left\langle u, w_{jk,\ell} \right\rangle_{L_2(c_\ell\Omega_T, \gamma_\ell)} w_{jk,\ell} \\ & \stackrel{(2.4)}{=} \sum_{j,k \in \mathbb{Z}} (1 + \beta_{\ell,T}|(j', k')|^2)^{-s/2} \left\langle u, w_{jk,\ell}^{(s)} \right\rangle_{H^s(c_\ell\Omega_T, \gamma_\ell)} w_{jk,\ell} \\ & \stackrel{(3.2)}{=} \sum_{j,k \in \mathbb{Z}} \left\langle u, w_{jk,\ell}^{(s)} \right\rangle_{H^s(c_\ell\Omega_T, \gamma_\ell)} w_{jk,\ell}^{(s)}, \end{aligned}$$

which yields completeness of $\{w_{jk,\ell}^{(s)}\}_{j,k \in \mathbb{Z}}$ in $H^s(c_\ell\Omega_T, \gamma_\ell)$ and concludes the proof. \square

Due to the above result, every $\phi_\ell \in H^s(c_\ell\Omega_T, \gamma_\ell)$ can be written in the form

$$\phi_\ell = \sum_{j,k \in \mathbb{Z}} \phi_{jk,\ell} w_{jk,\ell}^{(s)}, \quad \text{where} \quad \phi_{jk,\ell} := \left\langle \phi_\ell, w_{jk,\ell}^{(s)} \right\rangle_{H^s(c_\ell\Omega_T, \gamma_\ell)}, \quad (3.3)$$

and thus for an arbitrary turbulence $\phi = (\phi_\ell)_{\ell=1}^L \in \mathcal{D}(\tilde{A}^{(s)})$ there holds

$$\phi = \left(\sum_{j,k \in \mathbb{Z}} \phi_{jk,\ell} w_{jk,\ell}^{(s)} \right)_{\ell=1}^L.$$

Collecting the coefficients $\phi_{jk,\ell}$ into vectors $\phi_{jk} := (\phi_{jk,1}, \dots, \phi_{jk,L}) \in \mathbb{C}^L$ we obtain

Proposition 3.2. *Let the periodic atmospheric tomography operator $\tilde{A}^{(s)}$ be defined as in (3.1), let $w_{jk,\ell}^{(s)}$ be as in (3.2), and let the matrices $\tilde{A}_{jk} \in \mathbb{C}^{G \times L}$ be defined as*

$$\tilde{A}_{jk}^{(s)} := \left((2T)w_{jk,\ell}^{(s)}(\alpha_g^x h_\ell, \alpha_g^y h_\ell) \right)_{g,\ell=1}^{G,L}. \quad (3.4)$$

Then for all $\phi \in \mathcal{D}(\tilde{A}^{(s)})$ there holds

$$(\tilde{A}^{(s)}\phi)(x, y) = \sum_{j,k \in \mathbb{Z}} (\tilde{A}_{jk}^{(s)}\phi_{jk})w_{jk}(x, y). \quad (3.5)$$

Proof. The proof of this proposition follows the lines of [27, Proposition 4.1]: From the definition of $\tilde{A}^{(s)}$ and with the coefficient expansion (3.3) it follows that

$$\begin{aligned} (\tilde{A}_g^{(s)}\phi)(x, y) &= \sum_{\ell=1}^L \phi_\ell(c_\ell x + \alpha_g^x h_\ell, c_\ell y + \alpha_g^y h_\ell) \\ &\stackrel{(3.3)}{=} \sum_{\ell=1}^L \sum_{j,k \in \mathbb{Z}} \phi_{jk,\ell} w_{jk,\ell}^{(s)}(c_\ell x + \alpha_g^x h_\ell, c_\ell y + \alpha_g^y h_\ell) \\ &\stackrel{(2.5),(3.2)}{=} \sum_{\ell=1}^L \sum_{j,k \in \mathbb{Z}} \phi_{jk,\ell} (2T)w_{jk}(x, y)w_{jk,\ell}^{(s)}(\alpha_g^x h_\ell, \alpha_g^y h_\ell) \\ &\stackrel{(3.4)}{=} \sum_{j,k \in \mathbb{Z}} (\tilde{A}_{jk}^{(s)}\phi_{jk})_g w_{jk}(x, y), \end{aligned}$$

which yields (3.5). Note that the interchanging of series in the last line is justified since the norm of all the matrices $\tilde{A}_{jk}^{(s)}$ is bounded independently of j and k . \square

Following [27, 34], we now consider SVDs of the matrices $\tilde{A}_{jk}^{(s)}$. For all $j, k \in \mathbb{Z}$, let $r_{jk}^{(s)}$ denote the rank of $\tilde{A}_{jk}^{(s)}$, and let $u_{jk,n}^{(s)} \in \mathbb{C}^G$, $v_{jk,n}^{(s)} \in \mathbb{C}^L$, and $\sigma_{jk,n}^{(s)} \in \mathbb{R}^+$, $n = 1, \dots, r_{jk}^{(s)} \leq \min\{G, L\}$ be the singular vectors and values of $\tilde{A}_{jk}^{(s)}$ satisfying

$$\begin{aligned} \tilde{A}_{jk}^{(s)}\phi_{jk} &= \sum_{n=1}^{r_{jk}^{(s)}} \sigma_{jk,n}^{(s)} \left((v_{jk,n}^{(s)})^H \phi_{jk} \right) u_{jk,n}^{(s)}, \\ (v_{jk,m}^{(s)})^H v_{jk,n}^{(s)} &= \delta_{mn}, \quad (u_{jk,m}^{(s)})^H u_{jk,n}^{(s)} = \delta_{mn}, \\ \sigma_{jk,1}^{(s)} &\geq \sigma_{jk,2}^{(s)} \geq \dots \geq \sigma_{jk,n}^{(s)} > 0, \end{aligned} \quad (3.6)$$

where the the superscript H denotes the Hermitian of a matrix. Combining Proposition 3.2 with these SVDs (3.6) we obtain the following SVTD of $\tilde{A}^{(s)}$:

$$(\tilde{A}^{(s)}\phi)(x, y) = \sum_{j,k \in \mathbb{Z}} \left(\sum_{n=1}^{r_{jk}^{(s)}} \sigma_{jk,n}^{(s)} \left((v_{jk,n}^{(s)})^H \phi_{jk} \right) u_{jk,n}^{(s)} \right) w_{jk}(x, y). \quad (3.7)$$

As a result, we obtain an expression for the Moore-Penrose inverse $(\tilde{A}^{(s)})^\dagger$ of $\tilde{A}^{(s)}$.

Theorem 3.3. For $s \geq 0$ let the periodic atmospheric tomography operator $\tilde{A}^{(s)}$ be defined as in (3.1) and let (3.7) be its SVTD. Furthermore, let $\varphi \in L_2(\Omega_T)^G$ with

$$\varphi = \sum_{j,k \in \mathbb{Z}} \varphi_{jk} w_{jk}, \quad \text{where} \quad \varphi_{jk} = \left(\langle \varphi_g, w_{jk} \rangle_{L_2(\Omega_T)} \right)_{g=1}^G \in \mathbb{C}^G.$$

Then the best approximate solution of the equation $\tilde{A}^{(s)}\phi = \varphi$ is given by

$$((\tilde{A}^{(s)})^\dagger \varphi)_\ell(x, y) := \sum_{j,k \in \mathbb{Z}} \left(\sum_{n=1}^{r_{jk}^{(s)}} \frac{\left((u_{jk,n}^{(s)})^H \varphi_{jk} \right)}{\sigma_{jk,n}^{(s)}} v_{jk,n}^{(s)} \right)_\ell w_{jk,\ell}^{(s)}(x, y), \quad (3.8)$$

which is well-defined if and only if the following Picard condition holds:

$$\sum_{j,k \in \mathbb{Z}} \sum_{n=1}^{r_{jk}^{(s)}} \frac{|(u_{jk,n}^{(s)})^H \varphi_{jk}|^2}{(\sigma_{jk,n}^{(s)})^2} < \infty.$$

Proof. Let $s \geq 0$ be arbitrary but fixed and recall from its definition (3.3) that

$$\phi_{jk} = (\phi_{jk,1}, \dots, \phi_{jk,L}) = \left(\left\langle \phi_\ell, w_{jk,\ell}^{(s)} \right\rangle_{H^s(c_\ell \Omega_T, \gamma_\ell)} \right)_{\ell=1}^L.$$

Inserting this into the decomposition (3.7) we find that

$$(\tilde{A}^{(s)}\phi)(x, y) = \sum_{j,k \in \mathbb{Z}} \sum_{n=1}^{r_{jk}^{(s)}} \sigma_{jk,n}^{(s)} \left((v_{jk,n}^{(s)})^H \left(\left\langle \phi_\ell, w_{jk,\ell}^{(s)} \right\rangle_{H^s(c_\ell \Omega_T, \gamma_\ell)} \right)_{\ell=1}^L \right) u_{jk,n}^{(s)} w_{jk}(x, y),$$

which can be rewritten as

$$(\tilde{A}^{(s)}\phi)(x, y) = \sum_{j,k \in \mathbb{Z}} \sum_{n=1}^{r_{jk}^{(s)}} \sigma_{jk,n}^{(s)} \left\langle \phi, \left((v_{jk,n}^{(s)})_\ell w_{jk,\ell}^{(s)} \right)_{\ell=1}^L \right\rangle_{\mathcal{D}(\tilde{A}^{(s)})} u_{jk,n}^{(s)} w_{jk}(x, y).$$

This implies the following nullspace and range characterizations

$$\begin{aligned} \mathcal{N}(\tilde{A}^{(s)})^\perp &= \text{span} \left\{ \left((v_{jk,n}^{(s)})_\ell w_{jk,\ell}^{(s)} \right)_{\ell=1}^L \mid j, k \in \mathbb{Z}, 1 \leq n \leq r_{jk}^{(s)} \right\}, \\ \overline{\mathcal{R}(\tilde{A}^{(s)})} &= \text{span} \left\{ u_{jk,n}^{(s)} w_{jk} \mid j, k \in \mathbb{Z}, 1 \leq n \leq r_{jk}^{(s)} \right\}. \end{aligned} \quad (3.9)$$

and thus a candidate for a singular system of $\tilde{A}^{(s)}$ is given by

$$\left(\sigma_{jk,n}^{(s)}, \left((v_{jk,n}^{(s)})_\ell w_{jk,\ell}^{(s)} \right)_{\ell=1}^L, u_{jk,n}^{(s)} w_{jk} \right).$$

To show that this is indeed a singular system, we need to show three properties:

- (i) $\left\{ \left((v_{jk,n}^{(s)})_\ell w_{jk,\ell}^{(s)} \right)_{\ell=1}^L \mid j, k \in \mathbb{Z}, 1 \leq n \leq r_{jk}^{(s)} \right\}$ is an orthonormal system,
- (ii) $\left\{ u_{jk,n}^{(s)} w_{jk} \mid j, k \in \mathbb{Z}, 1 \leq n \leq r_{jk}^{(s)} \right\}$ is an orthonormal system,
- (iii) for all $j, k \in \mathbb{Z}$ and $1 \leq n \leq r_{jk}^{(s)}$ there holds

$$\tilde{A}^{(s)} \left((v_{jk,n}^{(s)})_\ell w_{jk,\ell}^{(s)} \right)_{\ell=1}^L = \sigma_{jk,n}^{(s)} u_{jk,n}^{(s)} w_{jk}.$$

For this, let $j, j', k, k' \in \mathbb{Z}$ and $1 \leq n \leq r_{jk}^{(s)}, 1 \leq n' \leq r_{j'k'}^{(s)}$ be arbitrary but fixed. Using the orthonormality of the functions $w_{jk,\ell}^{(s)}$ on $H^s(c_\ell \Omega_T, \gamma_\ell)$ we obtain

$$\begin{aligned} & \sum_{\ell=1}^L \left\langle (v_{jk,n}^{(s)})_\ell w_{jk,\ell}^{(s)}, (v_{j'k',n'}^{(s)})_\ell w_{j'k',\ell}^{(s)} \right\rangle_{H^s(c_\ell \Omega_T, \gamma_\ell)} \\ &= \sum_{\ell=1}^L (v_{jk,n}^{(s)})_\ell \overline{(v_{j'k',n'}^{(s)})_\ell} \left\langle w_{jk,\ell}^{(s)}, w_{j'k',\ell}^{(s)} \right\rangle_{H^s(c_\ell \Omega_T, \gamma_\ell)} \\ &= \left(v_{j'k',n'}^{(s)} \right)^H v_{jk,n}^{(s)} \delta_{jk,j'k'} = \delta_{n,n'} \delta_{jk,j'k'}, \end{aligned}$$

which establishes (i). Property (ii) can be shown analogously, and property (iii) follows directly from (3.9) using the orthonormality established in (i). Hence, we can apply the same arguments as in [14, Theorem 2.8], which then yield the assertion. \square

As mentioned before, the above analysis generalizes results of [34, 27], which were in particular derived for the case $s = 0$. In the case of only NGS, i.e., when $c_\ell = 1$ for all $\ell = 1, \dots, L$, the corollary below provides an explicit relation between the general case $s > 0$ and this base setting.

Corollary 3.4. *Let $s \geq 0$, let the operators $\tilde{A}^{(s)}, \tilde{A}^{(0)}$ be defined as in (3.1), and let $c_\ell = 1$ for all $\ell = 1, \dots, L$ (pure NGS case). Furthermore, let $(\sigma_{jk,n}^{(s)}, u_{jk,n}^{(s)}, v_{jk,n}^{(s)})$ and $(\sigma_{jk,n}^{(0)}, u_{jk,n}^{(0)}, v_{jk,n}^{(0)})$ denote the singular systems of the matrices $\tilde{A}_{jk}^{(s)}$ and $\tilde{A}_{jk}^{(0)}$ defined in (3.4), respectively. Then $\beta_T := \beta_{\ell,T}$ is independent of ℓ and it follows that*

$$(\tilde{A}^{(s)} \phi)(x, y) = \sum_{j,k \in \mathbb{Z}} (1 + \beta_T |(j, k)|^2)^{-s} \left(\sum_{n=1}^{r_{jk}^{(0)}} \sigma_{jk,n}^{(0)} \left((v_{jk,n}^{(s)})^H \phi_{jk} \right) u_{jk,n}^{(0)} \right) w_{jk}(x, y),$$

as well as

$$((\tilde{A}^{(s)})^\dagger \varphi)_\ell(x, y) = \sum_{j,k \in \mathbb{Z}} (1 + \beta_T |(j, k)|^2)^s \left(\sum_{n=1}^{r_{jk}^{(0)}} \frac{\left((u_{jk,n}^{(0)})^H \varphi_{jk} \right)}{\sigma_{jk,n}^{(0)}} v_{jk,n}^{(0)} \right)_\ell w_{jk,\ell}(x, y).$$

Proof. Note that due to (3.2) and (3.4) there holds

$$\tilde{A}_{jk}^{(s)} = (1 + \beta_T |(j, k)|^2)^{-s/2} \tilde{A}_{jk}^{(0)},$$

which implies that

$$\begin{aligned} (\tilde{A}_{jk}^{(s)})^H \tilde{A}_{jk}^{(s)} v_{jk,n}^{(0)} &= (1 + \beta_T |(j, k)|^2)^{-s} (\tilde{A}_{jk}^{(0)})^H \tilde{A}_{jk}^{(0)} v_{jk,n}^{(0)} \\ &= (1 + \beta_T |(j, k)|^2)^{-s} (\sigma_{jk,n}^{(0)})^2 v_{jk,n}^{(0)}, \end{aligned}$$

and thus $\sigma_{jk,n}^{(s)} = (1 + \beta_T |(j, k)|^2)^{-s/2} \sigma_{jk,n}^{(0)}$, $r_{jk}^{(s)} = r_{jk}^{(0)}$ and $v_{jk,n}^{(s)} = v_{jk,n}^{(0)}$. Similarly, we obtain $u_{jk,n}^{(s)} = u_{jk,n}^{(0)}$ which together with (3.5) and (3.8) yields the assertion. \square

Note that the above corollary not only connects the SVTDs of $\tilde{A}^{(s)}$ in the pure NGS-case for different values of s , but also sheds some additional light on the ill-posedness of the problem. In particular, due to the factors $(1 + \beta_T |(j, k)|^2)^{-s}$, which essentially correspond to the singular values of the Sobolev embedding operator (cf. [29]), the inversion of $\tilde{A}^{(s)}$ is ill-posed for each $s > 0$. Furthermore, if (2.6) holds, then the degree of ill-posedness is exactly $s/2$, i.e., the same as for the problem of inverting the Sobolev embedding operator. However, if (2.6) is not satisfied, then the degree of ill-posedness may be significantly worse. Note that due to a result by Kolmogorov [30], a typical atmospheric turbulence layer is expected to satisfy $s = 11/6$. Note that this assumption is commonly used both for the simulation of atmospheric turbulence profiles [16, 31] as well as in modern reconstruction algorithms for atmospheric tomography; see e.g. [2, 15, 60].

3.1 Computational Aspects

In this section, we discuss some computational aspects which are relevant for the successful practical application of the SVDs derived above. First, recall that the atmospheric tomography problem is generally ill-posed problem, and thus some form of regularization is required in case of noisy data φ^δ , which is always to be expected in practice. For this, one can employ a regularizing filter $g_\alpha : \mathbb{R} \rightarrow \mathbb{R}$ (cf. [14]) in the generalized inversion formula (3.8) to obtain the regularized solution

$$\phi_\alpha^\delta := \sum_{j,k \in \mathbb{Z}} \left(\sum_{n=1}^{r_{jk}^{(s)}} g_\alpha \left(\sigma_{jk,n}^{(s)} \right) \left((u_{jk,n}^{(s)})^H \varphi_{jk}^\delta \right) v_{jk,n}^{(s)} \right)_\ell w_{jk,\ell}^{(s)}(x, y). \quad (3.10)$$

In order for this approach to become a regularization method, the filters g_α need to be chosen appropriately. In our numerical experiments below, we use a Tikhonov filter of the form $g_\alpha^{\text{Tikh}}(s) := s/(s^2 + \alpha)$ together with a suitably selected regularization parameter α . However, other filter functions and truncation can also be used [14]. In fact, the practical necessity of discretizing the infinite sums in (3.10) implies that truncation is always present as an additional regularization in any implementation.

For an efficient implementation of the regularized SVD (3.10), we suggest equidistant discretization grids on the square domains $c_\ell\Omega_T$ and Ω_T , respectively. This has the advantage that the coefficients (φ_{jk}^δ) and the outer sum over the indices j, k can then be effectively computed via the two-dimensional FFT and IFFT, respectively. Furthermore, note that for a fixed atmospheric tomography setup, the singular systems of the matrices $A_{jk}^{(s)}$ can be precomputed and stored, which is beneficial for the repeated application of the inversion formula as required in an actual AO setup. The resulting inversion algorithm is summarized in pseudo-code in Algorithm 1.

Algorithm 1 SVTD

Require: $\varphi_1^\delta, \dots, \varphi_G^\delta \in \mathbb{R}^{N \times N}$, $\alpha \in \mathbb{R}^+$, $s \in \mathbb{R}^+$

- 1: **for** $g = 1, \dots, G$ **do**
- 2: $(\varphi_{jk}^\delta)_g = \text{fft2}(\varphi_g^\delta)$
- 3: **end for**
- 4: **for** $j, k \in I = \{[-N/2] + 1, \dots, [N/2] - 1\}$ **do**
- 5: $[u_{jk,n}^{(s)}, \sigma_{jk,n}^{(s)}, v_{jk,n}^{(s)}] = \text{SVD}(\tilde{A}_{jk}^{(s)})$
- 6: $d_{jk,\ell} = \sum_{n=1}^{r_{jk}^{(s)}} \frac{\sigma_{jk,n}^{(s)}}{(\sigma_{jk,n}^{(s)})^2 + \alpha} \left((u_{jk,n}^{(s)})^H \varphi_{jk}^\delta \right) v_{jk,n}^{(s)}$
- 7: **end for**
- 8: **for** $\ell = 1, \dots, L$ **do**
- 9: $(\phi_\alpha^\delta)_\ell = \text{ifft2}((d_{jk,\ell})_{j,k \in I})$
- 10: **end for**
- 11: **return** $(\phi_\alpha^\delta)_1, \dots, (\phi_\alpha^\delta)_L \in \mathbb{R}^{N \times N}$

Note that in Algorithm 1 we have implicitly assumed that both the atmospheric turbulence ϕ and the wavefronts φ are periodic functions defined on the square domain Ω_T . In practice, wavefronts are typically only given on a subset $\Omega_A \subset \Omega_T$ corresponding to the telescope aperture, and thus need to be extended outside Ω_A . The effect of this extension was studied in [21], where it was found to produce only very minor errors in the reconstructions along the boundaries of the domains $c_\ell\Omega_T$. Thus, all wavefronts used in the numerical examples of Section 5 are extended by 0.

4 An Explicit Frame Decomposition

In this section, we return from the periodic atmospheric tomography operator (3.1) to the classic version (2.1). For this operator, no explicit SVD is currently known, one reason for which is that finding orthonormal basis functions for $L_2(\Omega_\ell, \gamma_\ell)$ which satisfy algebraic properties similar to those of $w_{jk,\ell}$ is difficult. A remedy for this was recently proposed in [27], where a frame decomposition (FD) with properties comparable to the SVD was derived. Frames can be seen as generalized bases which do not need to be orthogonal, and thus are generally more flexible. Before discussing

the FD of [27] and our present contribution further, we first need to recall some general background on frames, summarized from [27] and the seminal works [4, 5].

Definition 4.1. A family of functions $\{e_k\}_{k \in K}$ in a Hilbert space H is called a frame over H , if and only if there exist constants $0 < A \leq B < \infty$ such that

$$A\|f\|_H^2 \leq \sum_{k \in K} |\langle f, e_k \rangle_H|^2 \leq B\|f\|_H^2. \quad (4.1)$$

The constants A and B are called frame bounds, and the frame is called tight if $A = B$. Furthermore, for a given frame $\{e_k\}_{k \in K}$ the frame (analysis) operator F and its adjoint (synthesis operator) F^* are defined by

$$\begin{aligned} F : H &\rightarrow \ell_2(K), & f &\mapsto \{\langle f, e_k \rangle\}_{k \in K}, \\ F^* : \ell_2(K) &\rightarrow H, & a &\mapsto \sum_{k \in K} a_k e_k. \end{aligned}$$

Note that due to (4.1), the frame operator satisfies

$$\sqrt{A} \leq \|F\| = \|F^*\| \leq \sqrt{B},$$

and thus the so-called frame operator, defined by

$$Sf := F^*Ff = \sum_{k \in K} \langle f, e_k \rangle e_k, \quad (4.2)$$

is continuously invertible with $AI \leq S \leq BI$, which allows the following definition.

Definition 4.2. Let $\{e_k\}_{k \in K}$ be a frame over the Hilbert space H and define

$$\tilde{e}_k := S^{-1}e_k. \quad (4.3)$$

Then the family of functions $\{\tilde{e}_k\}_{k \in K}$ is called the *dual frame* of $\{e_k\}_{k \in K}$.

For an FD of the atmospheric tomography operator, we consider the functions

$$w_{jk,\ell g}(x, y) := w_{jk,\ell}(x, y)I_{\ell g}(x, y) = \frac{\sqrt{\gamma_\ell}}{c_{\ell,g}} w_{jk}((x, y)/c_{\ell,g})I_{\ell g}(x, y), \quad (4.4)$$

where $I_{\ell g}$ denotes the indicator function of the domain $\Omega_A(\alpha_g h_\ell)$, i.e.,

$$I_{\ell g}(x, y) := I_{\Omega_A(\alpha_g h_\ell)}(x, y), \quad (4.5)$$

and T in (2.5) is such that (2.3) holds. The functions $w_{jk,\ell g}$ do in fact form a frame:

Lemma 4.1. [27, Lemma 4.2, Proposition 4.3] *The family of functions $\{w_{jk}\}_{j,k \in \mathbb{Z}}$ forms a tight frame over $L_2(\Omega_A)$ with frame bounds $A = B = 1$, and the family of functions $\{w_{jk,\ell g}\}_{j,k \in \mathbb{Z}, g=1, \dots, G}$ forms a frame over $L_2(\Omega_\ell, \gamma_\ell)$ with $1 \leq A \leq B \leq G$.*

Following [27], an FD for the atmospheric tomography operator is now given by

$$(A\phi)(x, y) = (2T) \sum_{\ell=1}^L \sum_{j, k \in \mathbb{Z}} \left(\frac{\sqrt{\gamma_\ell}}{c_{\ell, g}} w_{jk} \left(\frac{\alpha_g h_\ell}{c_{\ell, g}} \right) \langle \phi_\ell, w_{jk, \ell g} \rangle_{L_2(\Omega_\ell, \gamma_\ell)} \right)_{g=1}^G w_{jk}(x, y). \quad (4.6)$$

Furthermore, similarly as for the SVD, one may define the operator

$$\begin{aligned} \mathcal{A} : L_2(\Omega_A)^G &\rightarrow \prod_{\ell=1}^L L_2(\Omega_\ell, \gamma_\ell) \\ \varphi &\mapsto (2T) \sum_{j, k \in \mathbb{Z}} \sum_{g=1}^G \left(\frac{\sqrt{\gamma_\ell}}{c_{\ell, g} \sigma_g^2} w_{jk} \left(-\frac{\alpha_g h_\ell}{c_{\ell, g}} \right) \langle \varphi_g, w_{jk} \rangle_{L_2(\Omega_A)^G} \tilde{w}_{jk, \ell g} \right)_{\ell=1}^L, \end{aligned} \quad (4.7)$$

where $\sigma_g := \sqrt{\sum_{\ell=1}^L \gamma_\ell c_{\ell, g}^{-2}}$. As in [27], the operator \mathcal{A} can be shown to be well-defined and bounded, and satisfies the following approximate solution properties.

Theorem 4.2. *Let the atmospheric tomography operator A be as in (2.1), let \mathcal{A} be defined as in (4.7), and let $\varphi \in L_2(\Omega_A)^G$. Furthermore, assume that the sequences*

$$a_\ell := \left\{ \frac{\sqrt{\gamma_\ell}}{c_{\ell, g} \sigma_g^2} w_{jk} \left(-\frac{\alpha_g h_\ell}{c_{\ell, g}} \right) \langle \varphi_g, w_{jk} \rangle_{L_2(\Omega_A)^G} \right\}_{j, k \in \mathbb{Z}, g=1, \dots, G}, \quad (4.8)$$

satisfy $a_\ell \in R(F_\ell)$ for all $\ell \in \{1, \dots, L\}$, where F_ℓ denotes the frame operator corresponding to the frame $\{w_{jk, \ell g}\}_{j, k \in \mathbb{Z}, g=1, \dots, G}$. Then $\mathcal{A}\varphi$ is a solution of the equation $A\phi = \varphi$. Furthermore, among all other solutions $\psi \in \mathcal{D}(A)$ of $A\phi = \varphi$ there holds

$$\sum_{g, \ell=1}^{G, L} \sum_{j, k \in \mathbb{Z}} \left| \langle (\mathcal{A}\varphi)_\ell, w_{jk, \ell g} \rangle_{L_2(\Omega_\ell, \gamma_\ell)} \right|^2 \leq \sum_{g, \ell=1}^{G, L} \sum_{j, k \in \mathbb{Z}} \left| \langle \psi_\ell, w_{jk, \ell g} \rangle_{L_2(\Omega_\ell, \gamma_\ell)} \right|^2.$$

On the other hand, assume that $A\phi = \varphi$ is solvable, and let ϕ^\dagger denote the minimum-norm solution. Then regardless of whether $a_\ell \in R(F_\ell)$ there holds

$$\mathcal{A}\varphi = \phi^\dagger + (\tilde{F}_\ell^* b_\ell)_{\ell=1}^L, \quad \text{with} \quad b_\ell := \left\{ \left(P_{N(B_{jk})} \phi_{jk}^\dagger \right)_{\ell+(g-1)L} \right\}_{j, k \in \mathbb{Z}, g=1, \dots, L},$$

where the vectors $\phi_{jk}^\dagger \in \mathbb{C}^{L \cdot G}$ and the matrices $B_{jk} \in C^{G \times (L \cdot G)}$ are defined by

$$\begin{aligned} \phi_{jk}^\dagger &:= \text{vec} \left\{ \left(\langle \phi^\dagger, w_{jk, \ell g} \rangle_{L_2(\Omega_\ell, \gamma_\ell)} \right)_{\ell=1}^L \right\}_{g=1}^G, \\ B_{jk} &:= \text{diag} \left\{ (2T) \left(\frac{\sqrt{\gamma_\ell}}{c_{\ell, g}} w_{jk} \left(\frac{\alpha_g h_\ell}{c_{\ell, g}} \right) \right)_{\ell=1}^L \right\}_{g=1}^G. \end{aligned}$$

Proof. These results were shown for $\gamma_\ell = 1$ in [27]; see in particular Theorem 4.8 and the subsequent remark. They can be obtained analogously for general γ_ℓ . \square

The definition (4.7) of the frame inverse \mathcal{A} involves the dual frame functions $\tilde{w}_{jk,\ell g}$, which had to be computed numerically in [27, 56]. However, we now show that these functions $\tilde{w}_{jk,\ell g}$ have a simple analytic expression, which in turn leads to an explicit representation of \mathcal{A} that does not involve infinite sums. For this, we denote the overlay functions of the ℓ -th atmospheric layer as

$$O_\ell(x, y) := \sum_{g=1}^G I_{\ell g}(x, y), \quad (4.9)$$

with $I_{\ell g}$ as in (4.5).

Lemma 4.3. *For fixed ℓ let $S_\ell := F_\ell^* F_\ell$, where F_ℓ denotes the frame operator corresponding to the frame $\{w_{jk,\ell g}\}_{j,k \in \mathbb{Z}, g=1, \dots, G}$. Then for all $f \in L_2(\Omega_\ell, \gamma_\ell)$ there holds*

$$S_\ell f(x, y) = f(x, y) O_\ell(x, y). \quad (4.10)$$

Proof. Let ℓ and $f \in L_2(\Omega_\ell, \gamma_\ell)$ be arbitrary but fixed and for $(x, y) \in c_{\ell, g} \Omega_T$ define

$$h(x, y) := \begin{cases} f(x, y) I_{\ell, g}(x, y), & (x, y) \in \Omega_\ell, \\ 0, & (x, y) \in (c_{\ell, g} \Omega_T) \setminus \Omega_\ell. \end{cases} \quad (4.11)$$

Since $f \in L_2(\Omega_\ell, \gamma_\ell)$ it follows that $h \in L^2(c_{\ell, g} \Omega_T, \gamma_\ell)$, and thus

$$\begin{aligned} h(x, y) &= \sum_{j, k \in \mathbb{Z}} \langle h, w_{jk, \ell} \rangle_{L^2(c_{\ell, g} \Omega_T, \gamma_\ell)} w_{jk, \ell}(x, y) \\ &= \sum_{j, k \in \mathbb{Z}} \langle f I_{\ell, g}, w_{jk, \ell} \rangle_{L^2(\Omega_\ell, \gamma_\ell)} w_{jk, \ell}(x, y). \end{aligned} \quad (4.12)$$

Hence, using the definition (4.2) of the operator S_ℓ we find that for all $(x, y) \in \Omega_\ell$,

$$\begin{aligned} S_\ell f(x, y) &= \sum_{g=1}^G \sum_{j, k \in \mathbb{Z}} \langle f, w_{jk, \ell g} \rangle_{L^2(\Omega_\ell, \gamma_\ell)} w_{jk, \ell g}(x, y) \\ &\stackrel{(2.5)}{=} \sum_{g=1}^G \sum_{j, k \in \mathbb{Z}} \langle f, w_{jk, \ell} I_{\ell g} \rangle_{L^2(\Omega_\ell, \gamma_\ell)} w_{jk, \ell}(x, y) I_{\ell g}(x, y) \\ &= \sum_{g=1}^G I_{\ell g}(x, y) \sum_{j, k \in \mathbb{Z}} \langle f I_{\ell g}, w_{jk} \rangle_{L^2(\Omega_\ell, \gamma_\ell)} w_{jk, \ell}(x, y) \\ &\stackrel{(4.12)}{=} \sum_{g=1}^G I_{\ell g}(x, y) h(x, y) \stackrel{(4.11)}{=} f(x, y) \sum_{g=1}^G I_{\ell g}(x, y)^2, \end{aligned}$$

which together with $I_{\ell, g}(x, y)^2 = I_{\ell, g}(x, y)$ and (4.9) yields the assertion. \square

Using this result, we obtain an explicit expression for the functions $w_{jk,\ell g}$.

Corollary 4.4. For fixed ℓ , let the frame functions $w_{jk,\ell g}$ be defined as in (4.4). Then for the dual frame functions $\tilde{w}_{jk,\ell g}$ of the frame $\{w_{jk,\ell g}\}_{j,k \in \mathbb{Z}, g=1, \dots, G}$ there holds

$$\tilde{w}_{jk,\ell g}(x, y) = w_{jk,\ell g}(x, y)/O_\ell(x, y), \quad \forall (x, y) \in \Omega_\ell. \quad (4.13)$$

Proof. Recall that by definition (4.3), there holds $\tilde{w}_{jk,\ell g} = S_\ell^{-1}w_{jk,\ell g}$. Hence, using (4.10) and the fact that O_ℓ is nonzero on Ω_ℓ directly yields the assertion. \square

For further considerations, we also require an expression for the adjoint of \mathcal{A} .

Lemma 4.5. Let the atmospheric tomography operator A be defined as in (2.1) with the FD given in (4.6). Then for the adjoints A_g^* of its components there holds

$$\begin{aligned} A_g^* : L_2(\Omega_A) &\rightarrow \mathcal{D}(A) = \prod_{\ell=1}^L L_2(\Omega_\ell, \gamma_\ell) \\ \varphi_g &\mapsto (2T) \sum_{j,k \in \mathbb{Z}} \frac{\sqrt{\gamma_\ell}}{c_{\ell,g}} \langle \varphi_g, w_{jk} \rangle_{L_2(\Omega_A)} w_{jk} \left(-\frac{\alpha_g h_\ell}{c_{\ell,g}} \right) w_{jk,\ell g} \end{aligned} \quad (4.14)$$

Proof. Using the FD (4.6) of the atmospheric tomography operator, we obtain

$$\begin{aligned} &\langle A_g \phi, \varphi_g \rangle_{L_2(\Omega_A)} \\ &= (2T) \sum_{j,k \in \mathbb{Z}} \sum_{\ell=1}^L \frac{\sqrt{\gamma_\ell}}{c_{\ell,g}} w_{jk} \left(\frac{\alpha_g h_\ell}{c_{\ell,g}} \right) \langle \phi_\ell, w_{jk,\ell g} \rangle_{L_2(\Omega_\ell, \gamma_\ell)} \langle w_{jk}, \varphi_g \rangle_{L_2(\Omega_A)} \\ &= \sum_{\ell=1}^L \left\langle \phi_\ell, (2T) \sum_{j,k \in \mathbb{Z}} \frac{\sqrt{\gamma_\ell}}{c_{\ell,g}} w_{jk} \left(-\frac{\alpha_g h_\ell}{c_{\ell,g}} \right) \langle \varphi_g, w_{jk} \rangle_{L_2(\Omega_A)} w_{jk,\ell g} \right\rangle_{L_2(\Omega_\ell, \gamma_\ell)}, \end{aligned}$$

for all $\varphi_g \in L_2(\Omega_A)$ and $\phi \in \mathcal{D}(A)$, which directly yields the assertion. \square

Using this representation of the adjoint atmospheric tomography operator, we can now find an explicit representation of the approximate solution operator \mathcal{A} .

Theorem 4.6. Let the operator \mathcal{A} be defined as in (4.7) and let $\varphi \in L_2(\Omega_A)^G$. Then

$$\begin{aligned} (\mathcal{A}\varphi)(r) &= \sum_{g=1}^G \left(\frac{\gamma_\ell}{(c_{\ell,g}\sigma_g)^2} \varphi_g \left(\frac{r - \alpha_g h_\ell}{c_{\ell,g}} \right) I_{\Omega_A(\alpha_g h_\ell)}(r)/O_\ell(r) \right)_{\ell=1}^L \\ &= \sum_{g=1}^G \left(\frac{1}{\sigma_g^2 O_\ell(r)} (A_g^* \varphi_g)(r) \right)_{\ell=1}^L. \end{aligned} \quad (4.15)$$

Proof. First, note that a comparison of the expressions (2.2) and (4.14) for A_g^* yields

$$\begin{aligned} &\frac{\gamma_\ell}{c_{\ell,g}^2} \varphi_g \left(\frac{r - \alpha_g h_\ell}{c_{\ell,g}} \right) I_{\Omega_A(\alpha_g h_\ell)}(r) \stackrel{(2.2)}{=} A_g^* \varphi_g \\ &\stackrel{(4.14)}{=} (2T) \sum_{j,k \in \mathbb{Z}} \frac{\sqrt{\gamma_\ell}}{c_{\ell,g}} \langle \varphi_g, w_{jk} \rangle_{L_2(\Omega_A)} w_{jk} \left(-\frac{\alpha_g h_\ell}{c_{\ell,g}} \right) w_{jk,\ell g}(r). \end{aligned}$$

Hence, dividing both sides by $\sigma_g^2 O_\ell(r)$ and summing over g , we find that

$$\begin{aligned} \sum_{g=1}^G \frac{\gamma_\ell}{\sigma_g^2 c_{\ell,g}^2} \varphi_g \left(\frac{r - \alpha_g h_\ell}{c_{\ell,g}} \right) I_{\Omega_A(\alpha_g h_\ell)}(r) / O_\ell(r) &= \sum_{g=1}^G \frac{1}{\sigma_g^2 O_\ell(r)} (A_g^* \varphi_g)(r) \\ &= (2T) \sum_{j,k \in \mathbb{Z}} \sum_{g=1}^G \frac{\sqrt{\gamma_\ell}}{\sigma_g^2 c_{\ell,g}} (\varphi_{jk})_g w_{jk} \left(-\frac{\alpha_g h_\ell}{c_{\ell,g}} \right) w_{jk,\ell g}(r) / O_\ell(r). \end{aligned}$$

Now, since due to (4.13) there holds $\tilde{w}_{jk,\ell g} = w_{jk,\ell g} / O_\ell$, the right side of the above expression equals the ℓ -th component of $\mathcal{A}\varphi$, cf. (4.7), which yields the assertion. \square

In Theorem 4.2, we have seen that the frame inverse $\mathcal{A}\varphi$ is a solution of $A\phi = \varphi$ if the sequences a_ℓ defined in (4.8) satisfy $a_\ell \in R(F_\ell)$ for all $\ell \in \{1, \dots, L\}$. However, this condition is difficult to verify, in particular since the ranges $R(F_\ell)$ are non-trivial subsets of $\ell_2(\mathbb{N})$. But if $a_\ell \notin R(F_\ell)$, then in general $\mathcal{A}\phi$ can only be expected to be an approximate solution in the sense of Theorem 4.2. A potential solution for this would be to project the frames $\{w_{jk}\}_{j,k \in \mathbb{Z}}$ and $\{w_{jk,\ell,g}\}_{j,k \in \mathbb{Z}, g=1, \dots, G}$ onto $\overline{R(A)}$ and $N(A)^\perp$, respectively [9, 28]. However, to do so analytically would essentially require an explicit form of the Moore-Penrose inverse A^\dagger of A , which is not available. Hence, in this paper we propose a remedy in the form of the *iterative FD*, given by

$$\phi_{k+1} = \phi_k + \mathcal{A}(\varphi - A\phi_k). \quad (4.16)$$

This method essentially amounts to fixed point iteration applied to the modified normal $\mathcal{A}A\phi = \mathcal{A}\varphi$, which we expect to converge to a solution of the atmospheric tomography operator satisfying the range condition $a_\ell \in R(F_\ell)$. While at the moment we cannot provide a full theoretical justification of this approach, the numerical results presented below demonstrate that the iterative FD significantly improves the quality of the obtained reconstructions. This is perhaps not very surprising, given that in Theorem 4.6 we have found that \mathcal{A} corresponds to a specifically weighted adjoint of A , and thus (4.16) is essentially a gradient method.

In fact, the gradient methods for the atmospheric tomography problem developed in [48] make use of the following adapted inner product on the atmospheric layers:

$$\langle \psi, \theta \rangle_\xi = \sum_{\ell=1}^L \frac{1}{\gamma_\ell} \int_{\Omega_\ell} O_\ell(r) \psi_\ell(r) \overline{\theta_\ell(r)} dr.$$

The adjoint of the atmospheric tomography operator with respect to this weighted inner product then takes the form

$$(A_\xi^* \varphi)(r) = \sum_{g=1}^G (A_{g,\xi}^* \varphi)(r) = \sum_{g=1}^G \left(\frac{\gamma_\ell}{c_{\ell,g}^2} \varphi_g \left(\frac{r - \alpha_g h_\ell}{c_{\ell,g}} \right) I_{\Omega_A(\alpha_g h_\ell)}(r) / O_\ell(r) \right)_{l=1}^L.$$

Comparing this with (4.7), we find that $\mathcal{A} = \sum_{g=1}^G \sigma_g^2 A_{g,\xi}^*$, providing another link between the iterative FD (4.16) and the specific gradient methods derived in [48].

5 Numerical Experiments

In this section, we give some numerical verification of our developed algorithms. To this end, we consider realistic AO systems motivated by the ELT, which is currently under construction in the Atacama desert in Chile. We first describe the test configurations and simulation environment in detail, and then compare the proposed methods with state of the art algorithms in terms of reconstruction quality.

5.1 Test Configuration and Simulation Environment

To evaluate the performance of the proposed algorithms, we use a design similar to that of the ELT, which will become the largest optical/near-infrared telescope in the world. The ELT will be equipped with two so-called Nasmyth platforms on each side containing different instruments. The test setting in this paper is motivated by the instrument MORFEO [7], which is an AO module operating in MCAO.

The AO system configuration is shown in Table 5.1. We simulate a telescope which gathers light through a primary mirror with 42 m diameter and a 28% central obstruction. The ELT optical design consists of three mirrors denoted by M1, M2 and M3 on-axis with two DMs (M4, M5) for performing the AO. For MORFEO, two additional DMs (DM1, DM2) inside the instrument are used for wavefront compensation. Note that we assume the Fried geometry with equidistant actuator spacing for all DMs [18]. Details on the configuration are listed in Table 5.2. The turbulence is simulated according to median seeing conditions with a Fried parameter of 0.129 m. We use the ESO standard 9-layer atmosphere as e.g. defined in [3] and reconstruct 3 layers at the altitudes of the DMs, see Table 5.3. Figure 5.1 shows a graphical illustration of the DM and layer configuration. The layer heights are chosen such that the light emitted from a certain turbulent layer is exactly focused in the corresponding DM. A wavefront perturbation stemming from one of these layers, which are assumed to be infinitely thin, is then exactly compensated if the corresponding DM is given the correct shape. This special choice of the mirror position along the optical axis is often referred to as conjugation. In this way, we obtain the DM shapes directly from the reconstructed layers and do not have to perform a projection step.

We test our algorithms on two different configurations of natural guide stars (NGS) and laser guide stars (LGS) for measuring the wavefront aberrations, see Figure 5.2. In the first test case (Figure 5.2, left) we simulate 6 bright NGS positioned in a circle of 1 arcmin diameter. This setting is easier to handle, as the modelling of LGS is more complex due to their finite height. Moreover, wavefronts obtained by LGS face the problem of tip-tilt indetermination [44], i.e., the planar component of the measured wave is unreliable. In practice, it is not realistic to find 6 bright NGS in the surrounding of the object of interest. Thus, we consider as second test configuration (Figure 5.2, right) the standard MORFEO setting with 6 LGS positioned in a circle of 1 arcmin diameter. We account for the tip-tilt effect via removing the planar component of LGS wavefronts using 3 faint NGS located in a circle of 160 arcsec diameter [22]. We model the sodium layer at which the LGS

Parameter	Value
Telescope diameter	42 m
Central obstruction	28%
Fried parameter r_0	0.129 m
Na-layer height	90 km
Na-layer FWHM	11.4 km
Field of View	2 arcmin
Evaluation criterion	Strehl ratio
Evaluation wavelength	K band (2200 nm)

Table 5.1: General system parameters.

	M4	DM1	DM2
Actuators	85×85	47×47	53×53
Altitude	0 km	4 km	12.7 km
Spacing	0.5 m	1 m	1 m

Table 5.2: DM configuration.

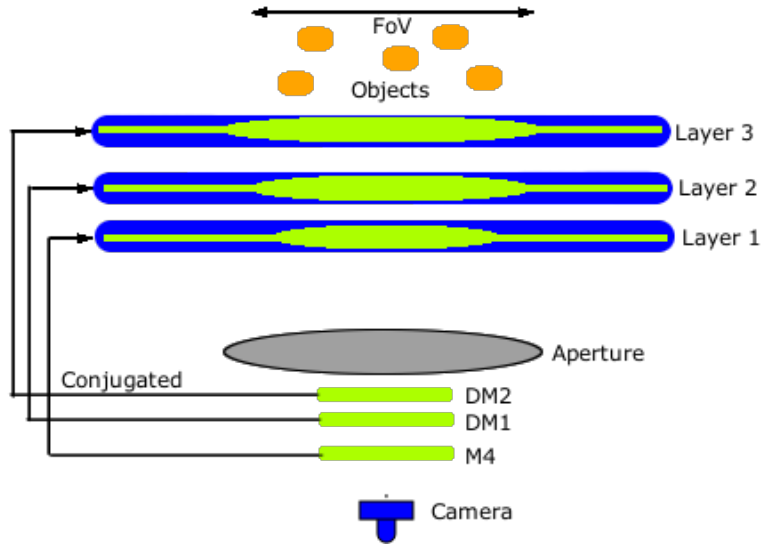


Figure 5.1: Graphical illustration of 3 DMs conjugated to 3 reconstructed layers.

beam is scattered via a Gaussian random variable with mean altitude $H = 90$ km and FWHM of the sodium density profile of 11.4 km. To each bright NGS and LGS, a Shack-Hartmann (SH) WFS with 84×84 subapertures is assigned. The faint NGS for tip-tilt removal are equipped with 2×2 SH WFS. The noise induced by the detector read-out is simulated as 3.0 electrons per pixel and frame. A detector read-out noise (RON) of 3.0 electrons per pixel per frame is used. For more details see Table 5.4.

We examine the performance of the proposed methods against the Gradient method [48, 47] and the Finite Element Wavelet Hybrid Algorithm (FEWHA) [58, 60], both being iterative reconstruction algorithms for atmospheric tomography. FEWHA uses a dual-domain discretization strategy into wavelet and bilinear basis functions leading to sparse operators. A matrix-free representation of all operators involved makes FEWHA very fast and enables on-the-fly system updates whenever parameters at the telescope or in the atmosphere change [50, 49]. The sparse system

Layer	Altitude	Strength
1	0 m	0.75
2	4000 m	0.15
3	12700 m	0.1

Table 5.3: Layer configuration.

	LGS-WFS	NGS-WFS	TT-WFS
Type	SH WFS	SH WFS	SH WFS
Subap.	84×84	84×84	2×2
Wavelength	589 nm	589 nm	1650 nm

Table 5.4: WFS configuration.

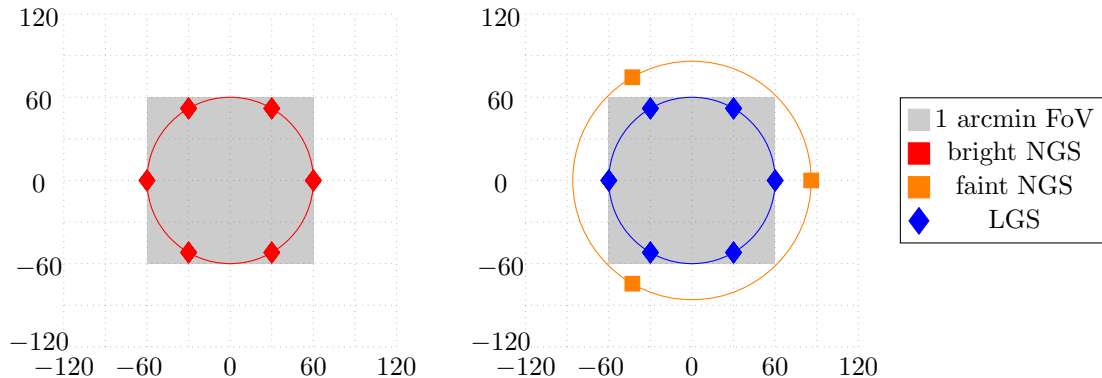


Figure 5.2: Different configurations of bright (red) and faint (orange) NGSs and LGSs (blue). The 2 arcmin FoV is marked in gray.

is solved using the CG method with a Jacobi preconditioner [59] and an augmented Krylov subspace method [41, 49] to reduce the number of iterations. The algorithm leads in real-time to an excellent reconstruction quality compared to standard matrix-vector multiplication approaches for the MORFEO instrument [49, 51]. The Gradient method amounts to a steepest descent method applied to a least squares functional, employed with an accelerated step-size, developed and analyzed in [48, 47], here applied with a separated tip-tilt reconstruction in the mixed case.

In the community of AO, it is common to validate the reconstruction quality using the so called Strehl ratio into certain directions [44]. In our simulations, we use 25 directions positioned in a 5×5 grid over the FoV. The Strehl ratio is defined as the ratio between the maximum of the real energy distribution of incoming light in the image plane $I(x, y)$ over the hypothetical distribution $I_D(x, y)$, which stems from the assumption of diffraction-limited imaging, i.e.,

$$\text{SR} := \frac{\max_{(x,y)} I(x, y)}{\max_{(x,y)} I_D(x, y)}.$$

By definition, the Strehl ratio is between 0 and 1 and frequently given in percent. A Strehl ratio of 1 means that the influence of the atmosphere has been removed from the observation. For its numerical evaluation the Marechal criterion is used [44].

For our SVTD method summarized in Algorithm 1, we used $s = 1$ for the Sobolev index, which is slightly smaller than the choice $s = 11/6$ corresponding to the expected smoothness of a typical atmosphere [30]. This was done to avoid the commonly observed oversmoothing effect of the adjoint embedding operator [29, 40].

All simulations have been carried out in the internal and entirely MATLAB-based AO simulation tool MOST [2], which has been developed by the Austrian Adaptive Optics team as an alternative to OCTOPUS [32, 16], the end-to-end simulator of the European Southern Observatory. The performance of the algorithms is evaluated using the Strehl ratio in the K band, i.e., at a wavelength of 2200 nm.

5.2 Numerical Results

As a first step of performance evaluation, we consider not a whole end-to-end AO simulation, but compare only the tomographic reconstruction of the proposed methods. We simulate a 3 layer atmosphere (Figure 5.3, top row) and perform its reconstruction with the SVTD (Figure 5.3, middle row) and the iterative FD (Figure 5.3, bottom row) methods. We observe that both algorithms provide a very good result at the lowest layer $\ell = 1$, but fail to reconstruct details at higher altitudes, in particular around the borders. This behaviour is expected, and generally observed for atmospheric tomography, since the reconstruction quality depends on the number of overlapping regions, which decreases with height and with a larger distance from the center, which is often referred to as field off-axis position [42].

Since all algorithms yield promising tomographic reconstructions, we next consider full end-to-end AO simulations and evaluate the short-exposure (SE) and long-exposure (LE) Strehl ratio. The SE Strehl ratio provides a measure for the reconstruction quality at the current time step, whereas the LE Strehl ratio is an average over time [44]. We compare the SVTD and FD approaches with FEWHA and the Gradient method, which are both known to provide very good results for the considered test configurations. For all results with the SVTD method, the regularization parameter α and the smoothing parameter s were tuned experimentally a-priori. The results for the iterative FD and the Gradient method use 5 iterations, whereas FEWHA uses 4 iterations in its internal CG method. The method specific parameters for FEWHA have been tuned via simulations.

First, we consider the NGS-only case as illustrated in the left plot of Figure 5.2. We simulate 1000 time steps, corresponding to a 2 seconds interval. In Figure 5.4, we show the average SE Strehl ratio over the 25 evaluation directions over time (left) and the LE Strehl ratio versus the field off-axis position (right). Note that it is a well known issue for MCAO systems that the quality of the AO correction degrades if we move further away from the center, see e.g. [42]. We observe that all methods except the FD provide very good results, which are stable over time. In particular, the SVTD can compete with the Gradient method and FEWHA, even outperforming them in the center of the FoV. This also becomes evident when looking at the SE Strehl ratio at specific directions depicted Figure 5.5. The reason for the suboptimal performance of the FD is likely due to the assumptions on the sequences a_ℓ in Theorem 4.2 not being satisfied. Consistently with the discussion at the end of Section 4, the iterative FD performs much better than the FD itself, with results comparable to those of the Gradient method. Note that we did not focus on tuning the step-size in the iterative FD approach, which could possibly yield a

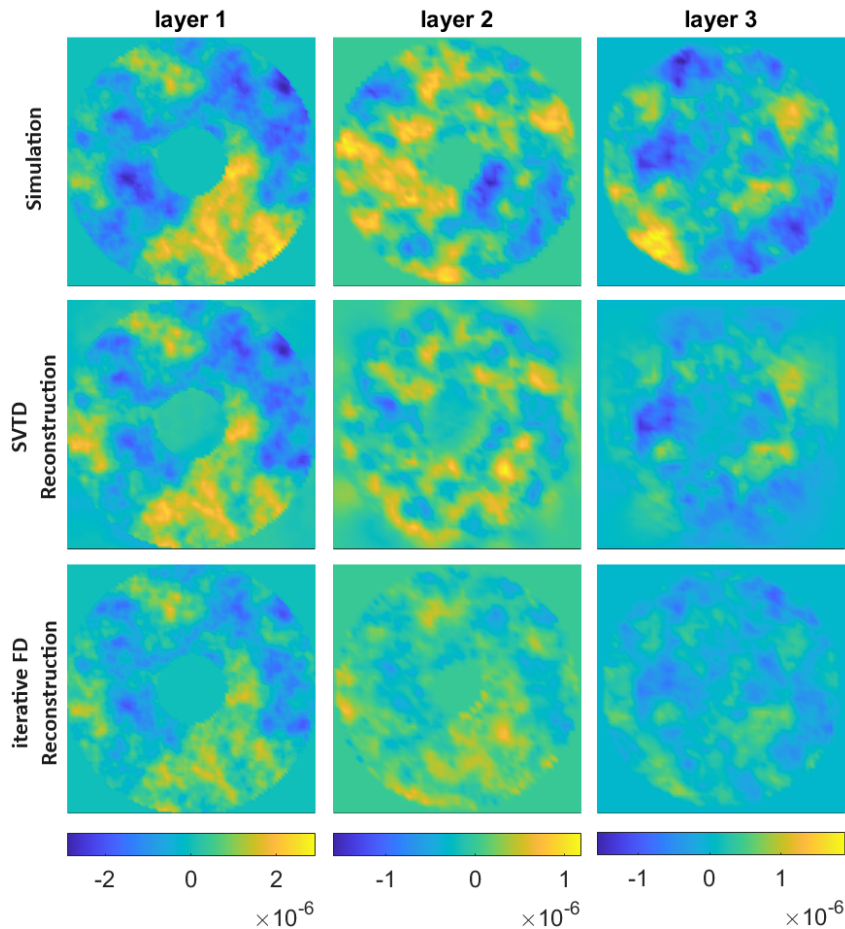


Figure 5.3: A simulated 3 layer atmosphere (top), and its reconstruction with SVTD (middle) and iterative FD (bottom).

performance improvement.

Next, we consider the more realistic mixed case in which 6 LGS are combined with 3 NGS for tip-tilt removal; cf. the right plot of Figure 5.2 for an illustration of the star asterism. We observe from Figure 5.6 and Figure 5.7 that FEWHA provides the best result in all directions considered over the whole simulation duration. In general, all algorithms yield more unstable results, i.e., oscillations of the SE Strehl ratio over time, especially for the outer directions. This is expected when moving from an NGS-only setting to a more realistic setting with LGS and faint NGS.

In terms of computational speed, the MATLAB implementations of all tested methods require a similar run-time, in the order of a few seconds for a single time step. Note that there exists a parallel and matrix-free implementation of FEWHA in C++, which takes only a few milliseconds per time step and thus is able to fulfill the real-time requirements of the ELT [50]. The FEWHA MATLAB implementation is matrix-based, non parallel and not optimized for speed, and thus much slower.

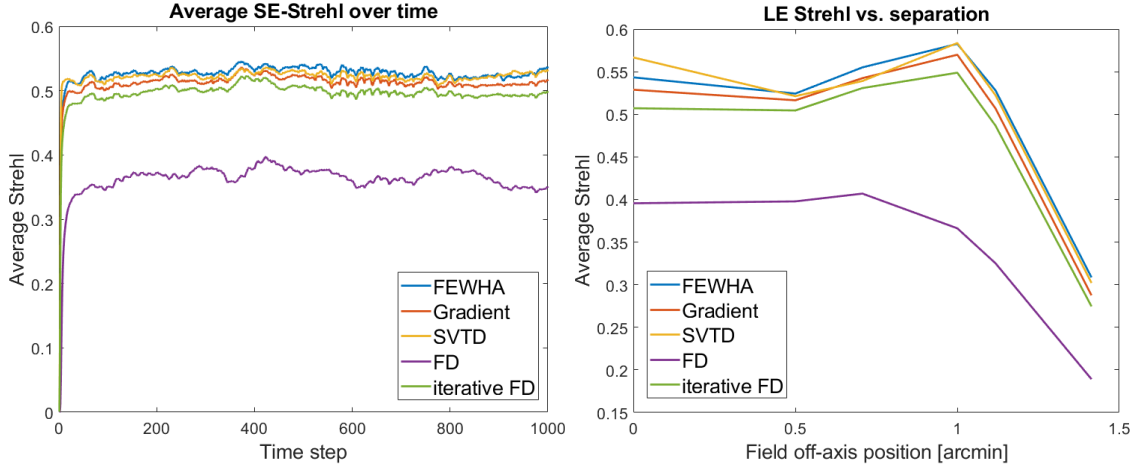


Figure 5.4: NGS-only case: Average SE Strehl ratio over time (left) and LE Strehl ratio vs. separation (right).

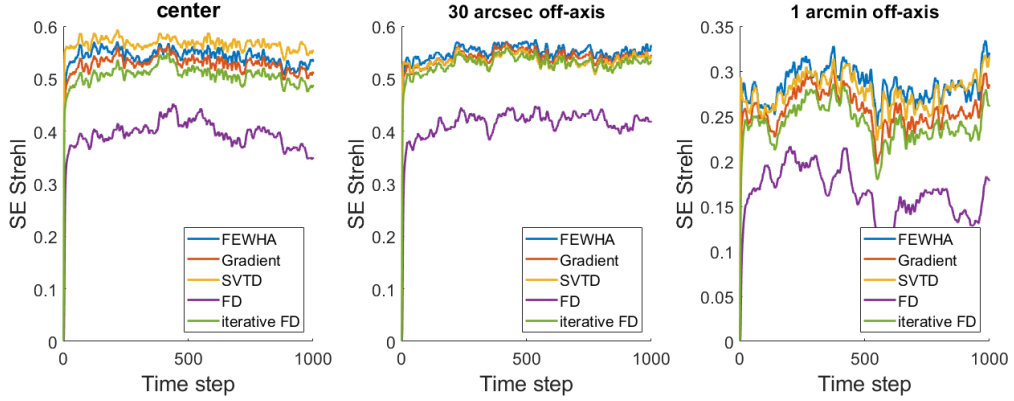


Figure 5.5: NGS-only case: SE Strehl ratio over time in the center (left), 30 arcsec off-axis (middle) and 1 arcmin off-axis (right).

6 Conclusion

In this paper, we considered singular value and frame decompositions of the atmospheric tomography operator. First, we extended existing SVDs for the periodic atmospheric tomography operator to a more realistic Sobolev space setting including weighted inner products which incorporate known or measured turbulence profiles. Then, we considered an FD for the non-periodic atmospheric tomography operator, and derived an explicit representation of the corresponding (approximate) frame inversion operator. Based on these theoretical results, we then developed efficient numerical solution methods for the atmospheric tomography problem, which we implemented and tested in the AO simulation tool MOST. The obtained results, especially those for the SVTD, are very promising, and warrant further investigation. In particular, we plan to implement the SVTD method in non-MATLAB based AO

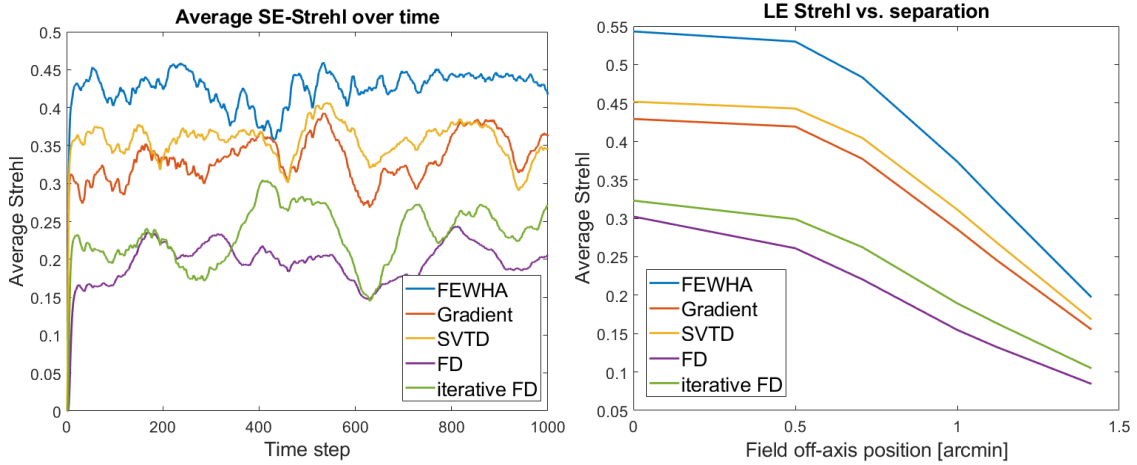


Figure 5.6: Mixed case: Average SE Strehl ratio over time (left) and LE Strehl ratio vs. separation (right).

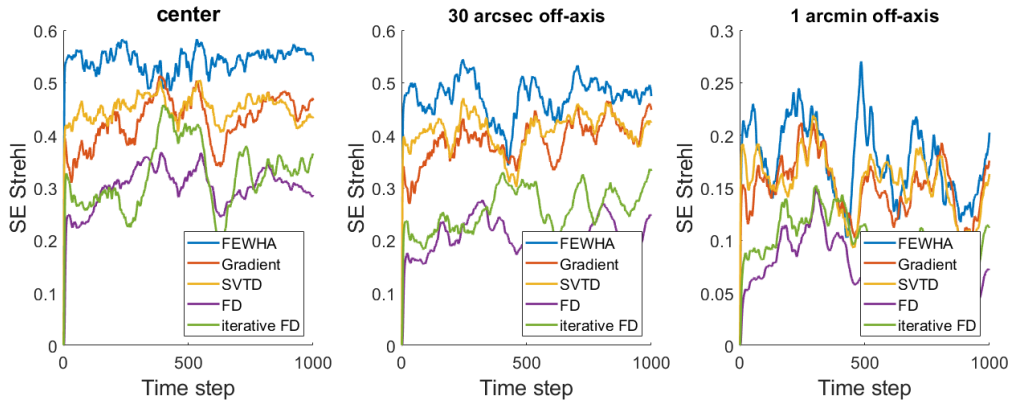


Figure 5.7: Mixed case: SE Strehl ratio over time in the center (left), 30 arcsec off-axis (middle) and 1 arcmin off-axis (right).

simulation environments, and to leverage its low computational cost and parallelizability to compete with the FEWHA algorithm not only in terms of reconstruction quality as demonstrated above, but also in essential real-time requirements.

Acknowledgement

The authors thank Andreas Obereder and Stefan Raffetseder for helpful input. This research was funded in part by the Austrian Science Fund (FWF) SFB 10.55776/F68 “Tomography Across the Scales”, project F6805-N36 (Tomography in Astronomy). For open access purposes, the authors have applied a CC BY public copyright license to any author-accepted manuscript version arising from this submission. Furthermore, the authors were supported by the Austrian Research Promotion Agency

(FFG) project number FO999888133, as well as the NVIDIA Corporation Academic Hardware Grant Program. LW is partially supported by the State of Upper Austria.

References

- [1] D. R. Andersen et al. “The MOAO system of the IRMOS near-Infrared Multi-Object Spectrograph for TMT”. In: *Proceedings of the SPIE*. Vol. 6269. Society of Photo-Optical Instrumentation Engineers (SPIE) Conference Series. 2006, 62694K. DOI: 10.1117/12.672177.
- [2] G. Auzinger. “New Reconstruction Approaches in Adaptive Optics for Extremely Large Telescopes”. PhD thesis. Johannes Kepler University Linz, 2017.
- [3] G. Auzinger. “On choosing layer profiles in atmospheric tomography”. In: *Journal of Physics: Conference Series* 595.1 (2015), p. 012001. DOI: 10.1088/1742-6596/595/1/012001. URL: <https://dx.doi.org/10.1088/1742-6596/595/1/012001>.
- [4] O. Christensen. *An Introduction to Frames and Riesz Bases*. Applied and Numerical Harmonic Analysis. Springer International Publishing, 2016. ISBN: 9783319256139.
- [5] I. Daubechies. *Ten Lectures on Wavelets*. Philadelphia, PA: Society for Industrial and Applied Mathematics, 1992. DOI: 10.1137/1.9781611970104. URL: <http://epubs.siam.org/doi/abs/10.1137/1.9781611970104>.
- [6] M. Davison. “The ill-conditioned nature of the limited angle tomography problem”. In: *SIAM J. Appl. Math.* 43 (1938), pp. 428–448.
- [7] E. Diolaiti et al. “MAORY: A Multi-conjugate Adaptive Optics Relay for the E-ELT”. In: *Messenger* (2010), 28–9.
- [8] E. Diolaiti et al. “MAORY: adaptive optics module for the E-ELT”. In: *Adaptive Optics Systems V*. Ed. by E. Marchetti, L. M. Close, and J.-P. Véran. Vol. 9909. International Society for Optics and Photonics. SPIE, 2016, pp. 768–774. DOI: 10.1117/12.2234585. URL: <https://doi.org/10.1117/12.2234585>.
- [9] A. Ebner, J. Friel, D. Lorenz, J. Schwab, and M. Haltmeier. “Regularization of inverse problems by filtered diagonal frame decomposition”. In: *Applied and Computational Harmonic Analysis* 62 (2023), pp. 66–83. DOI: 10.1016/j.acha.2022.08.005.
- [10] S. E. Egner. “Multi-Conjugate Adaptive Optics for LINC-NIRVANA. Laboratory tests of a Ground-Layer Adaptive Optics System and Vertical Turbulence Measurements at Mt. Graham.” PhD thesis. Combined Faculties for the Natural Sciences and for Mathematics of the Ruperto-Carola University of Heidelberg, 2006.
- [11] B. L. Ellerbroeck and C. R. Vogel. “Inverse problems in astronomical optics”. In: *Inverse Problems* 25.6 (2009), p. 063001.

- [12] B. Ellerbroek, L. Gilles, and C. Vogel. “A Computationally Efficient Wavefront Reconstructor for Simulation or Multi-Conjugate Adaptive Optics on Giant Telescopes”. In: *Proceedings of the SPIE*. Ed. by P. L. Wizinowich and D. Bonaccini. Vol. 4839. Society of Photo-Optical Instrumentation Engineers (SPIE) Conference Series. 2003, pp. 989–1000. DOI: 10.1117/12.459673.
- [13] B. L. Ellerbroek, L. Gilles, and C. R. Vogel. “Numerical simulations of multiconjugate adaptive optics wavefront reconstruction on giant telescopes”. In: *Appl. Optics* 42 (2003), pp. 4811–4818.
- [14] H. W. Engl, M. Hanke, and A. Neubauer. *Regularization of inverse problems*. English. Dordrecht: Kluwer Academic Publishers, 1996, pp. viii + 321. ISBN: 0-7923-4157-0.
- [15] M. Esclitzbichler, C. Pechstein, and R. Ramlau. “An H¹-Kaczmarz reconstructor for atmospheric tomography”. In: *Journal of Inverse and Ill-Posed Problems* 21 (June 2013). DOI: 10.1515/jip-2013-0007.
- [16] ESO. *Online description of OCTOPUS*. Tech. rep. URL: <http://www.eso.org/sci/facilities/develop/ao/tecno/octopus.html>.
- [17] European Southern Observatory (ESO). *ESO’s Extremely Large Telescope*. <https://www.eso.org/public/teles-instr/elt/>. Accessed: 2020-05-13.
- [18] D. L. Fried. “Least-square fitting a wave-front distortion estimate to an array of phase-difference measurements”. In: *J. Opt. Soc. Am.* 67.3 (1977), pp. 370–375. DOI: 10.1364/JOSA.67.000370. URL: <https://opg.optica.org/abstract.cfm?URI=josa-67-3-370>.
- [19] T. Fusco, J.-M. Conan, G. Rousset, L. M. Mugnier, and V. Michau. “Optimal wave-front reconstruction strategies for multi conjugate adaptive optics”. In: *J. Opt. Soc. Am. A* 18 (2001), pp. 2527–2538.
- [20] D. Gavel. “Tomography for multiconjugate adaptive optics systems using laser guide stars”. In: *Astronomical Telescopes and Instrumentation, no. 5490 in Proc. SPIE*. 2004, pp. 1356–1373.
- [21] D. Gerth, B. Hofmann, S. Birkholz, S. Koke, and G. Steinmeyer. “Regularization of an autoconvolution problem in ultrashort laser pulse characterization”. In: *Inverse Problems in Science and Engineering* 22.2 (2014), pp. 245–266. DOI: 10.1080/17415977.2013.769535.
- [22] L. Gilles and B. L. Ellerbroeck. “Split atmospheric tomography using laser and natural guide stars”. In: *J. Opt. Soc. Am.* 25 (2008), pp. 2427–2435.
- [23] L. Gilles, B. Ellerbroek, and C. Vogel. “A comparison of Multigrid V-cycle versus Fourier Domain Preconditioning for Laser Guide Star Atmospheric Tomography”. In: *Adaptive Optics: Analysis and Methods/Computational Optical Sensing and Imaging/Information Photonics/Signal Recovery and Synthesis Topical Meetings on CD-ROM, OSA Technical Digest (CD)*. Optical Society of America, 2007.

- [24] L. Gilles, B. Ellerbroek, and C. Vogel. “Layer-Oriented Multigrid Wavefront Reconstruction Algorithms for Multi-Conjugate Adaptive Optics”. In: *Proceedings of the SPIE*. Ed. by P. L. Wizinowich and D. Bonaccini. Vol. 4839. Society of Photo-Optical Instrumentation Engineers (SPIE) Conference Series. 2003, pp. 1011–1022. DOI: 10.1117/12.459347.
- [25] L. Gilles, B. L. Ellerbroek, and C. R. Vogel. “Preconditioned conjugate gradient wave-front reconstructors for multiconjugate adaptive optics”. In: *Applied Optics* 42.26 (2003), pp. 5233–5250.
- [26] F. Hammer et al. “The FALCON Concept: Multi-Object Spectroscopy Combined with MCAO in Near-IR”. In: *Scientific Drivers for ESO Future VLT/VLTI Instrumentation, ESO ASTROPHYSICS SYMPOSIA (European Southern Observatory)*. Ed. by J. Bergeron and G. Monnet. Berlin, Heidelberg: Springer, 2002, pp. 139–148. DOI: 10.1007/10857019_21.
- [27] S. Hubmer and R. Ramlau. “A frame decomposition of the atmospheric tomography operator”. In: *Inverse Problems* 36.9 (2020), p. 094001. DOI: 10.1088/1361-6420/aba4fe.
- [28] S. Hubmer, R. Ramlau, and L. Weissinger. “On regularization via frame decompositions with applications in tomography”. In: *Inverse Problems* 38.5 (2022), p. 055003. DOI: 10.1088/1361-6420/ac5b86.
- [29] S. Hubmer, E. Sherina, and R. Ramlau. “Characterizations of Adjoint Sobolev Embedding Operators with Applications in Inverse Problems”. In: *Electronic Transactions on Numerical Analysis* 59 (2023). Gold OA, pp. 116–144. DOI: 10.1553/etna_vol59s116.
- [30] A. N. Kolmogorov. *The local structure of turbulence in incompressible viscous fluid for very large reynolds numbers*. In Dokl. Akad. Nauk SSSR volume 30, pages 299–303. 1941.
- [31] M. Le Louarn, C. Vérinaud, V. Korkiakoski, N. Hubin, and E. Marchetti. “Adaptive optics simulations for the European Extremely Large Telescope”. In: *SPIE Astronomical Telescopes+ Instrumentation*. International Society for Optics and Photonics. 2006, pp. 627234–627234.
- [32] M. Le Louarn, C. Verinaud, V. Korkiakoski, N. Hubin, and E. Marchetti. “Adaptive optics simulations for the European Extremely Large Telescope - art. no. 627234”. In: *Advances in Adaptive Optics II, Prs 1-3*. Vol. 6272. 2006, U1048–U1056.
- [33] F. Natterer. *The Mathematics of Computerized Tomography*. Philadelphia, PA: Society for Industrial and Applied Mathematics, 2001. DOI: 10.1137/1.9780898719284.
- [34] A. Neubauer and R. Ramlau. “A Singular-Value-Type Decomposition for the Atmospheric Tomography Operator”. In: *SIAM Journal on Applied Mathematics* 77.3 (2017), pp. 838–853. DOI: 10.1137/16M108135X. URL: <https://doi.org/10.1137/16M108135X>.

- [35] M. Poettinger, R. Ramlau, and G. Auzinger. “A new temporal control approach for SCAO systems”. In: *Inverse Problems* 36 (2019), p. 015002.
- [36] M. Puech et al. “Coupling MOAO with integral field spectroscopy: specifications for the VLT and the E-ELT”. In: *Mon. Not. R. Astron. Soc.* 390 (2008), pp. 1089–1104.
- [37] S. Raffetseder, R. Ramlau, and M. Yudytskiy. “Optimal mirror deformation for multi conjugate adaptive optics systems”. In: *Inverse Problems* 32.2 (2016), p. 025009. URL: <http://stacks.iop.org/0266-5611/32/i=2/a=025009>.
- [38] R. Ramlau, A. Obereder, M. Rosensteiner, and D. Saxenhuber. “Efficient iterative tip/tilt reconstruction for atmospheric tomography”. In: *Inverse Problems in Science and Engineering* 22.8 (2014), pp. 1345–1366. DOI: 10.1080/17415977.2013.873534.
- [39] R. Ramlau and M. Rosensteiner. “An efficient solution to the atmospheric turbulence tomography problem using Kaczmarz iteration”. In: *Inverse Problems* 28 (2012), p. 095004.
- [40] R. Ramlau and G. Teschke. “Regularization of Sobolev Embedding Operators and Applications to Medical Imaging and Meteorological Data. Part I: Regularization of Sobolev Embedding Operators”. In: *Sampling Theory in Signal and Image Processing* 3.2 (2004), pp. 175–195.
- [41] R. Ramlau and B. Stadler. “An augmented wavelet reconstructor for atmospheric tomography”. In: *Electron. Trans. Numer. Anal.* 54 (2021), pp. 256–275. DOI: 10.1553/etna_vol154s256.
- [42] R. Ramlau and B. Stadler. *On some analytic properties of the atmospheric tomography operator: Non-Uniqueness and reconstructability issues*. 2024. arXiv: 2404.11126 [math.NA].
- [43] F. J. Rigaut, B. L. Ellerbroek, and R. Flicker. “Principles, limitations and performance of multiconjugate adaptive optics”. In: *Proc. SPIE* 4007 (2000), pp. 1022–1031.
- [44] F. Roddier. *Adaptive optics in astronomy*. Cambridge University Press, 1999.
- [45] M. C. Roggemann and B. Welsh. *Imaging through turbulence*. CRC Press laser, optical science, and technology series, CRC Press, 1996.
- [46] M. Rosensteiner and R. Ramlau. “The Kaczmarz algorithm for multi-conjugate adaptive optics with laser guide stars”. In: *J. Opt. Soc. Am.* 30 (2013), pp. 1680–1686.
- [47] D. Saxenhuber. “Gradient-based reconstruction algorithms for atmospheric tomography in Adaptive Optics systems for Extremely Large Telescopes”. 2016.
- [48] D. Saxenhuber and R. Ramlau. “A Gradient-based method for atmospheric tomography”. In: *Inverse Problems and Imaging* 10.3 (2016), pp. 781–805. DOI: <http://dx.doi.org/10.3934/ipi.2016022>.

- [49] B. Stadler. “Real-time computing methods for astronomical adaptive optics”. PhD thesis. Johannes Kepler Universität Linz, 2021.
- [50] B. Stadler, R. Biasi, M. Manetti, and R. Ramlau. “Parallel implementation of an iterative solver for atmospheric tomography”. In: (2021).
- [51] B. Stadler and R. Ramlau. “Performance of an iterative wavelet reconstructor for the Multi-conjugate Adaptive Optics Relay of the Extremely Large Telescope”. In: *Journal of Astronomical Telescopes, Instruments, and Systems* 8.2 (2022), p. 021503. DOI: 10.1117/1.JATIS.8.2.021503. URL: <https://doi.org/10.1117/1.JATIS.8.2.021503>.
- [52] M. Tallon et al. “Fractal iterative method for fast atmospheric tomography on extremely large telescopes”. In: *Adaptive Optics Systems II, no. 7736 in Proc. SPIE*. 2010, pp. 77360X–77360X–10.
- [53] M. Tallon et al. “Performances of MCAO on the E-ELT using the fractal iterative method for fast atmospheric tomography”. In: *Second International Conference on Adaptive Optics for Extremely Large Telescopes*. 2011, p. 63.
- [54] E. Thiébaud and M. Tallon. “Fast minimum variance wavefront reconstruction for extremely large telescopes”. In: *J. opt. Soc. Am. A* 27 (2010), pp. 1046–1059.
- [55] C. Vogel and Q. Yang. “Fast optimal wavefront reconstruction for multi-conjugate adaptive optics using the Fourier domain preconditioned conjugate gradient algorithm”. In: *Optics Express* 15 (2006), pp. 7487–7498.
- [56] L. Weissinger. “Realization of the Frame Decomposition of the Atmospheric Tomography Operator”. MA thesis. JKU Linz, 2021. URL: https://liss.jku.at/permalink/f/n2r1to/ULI_alma5185824070003340.
- [57] Q. Yang, C. R. Voge, and B. L. Ellerbroek. “Fourier domain preconditioned conjugate gradient algorithm for atmospheric tomography”. In: *Applied Optics* 45 (2006), pp. 5281–5293.
- [58] M. Yudytskiy. “Wavelet methods in adaptive optics”. PhD thesis. Johannes Kepler University Linz, Austria, 2014.
- [59] M. Yudytskiy, T. Helin, and R. Ramlau. “A frequency dependent preconditioned wavelet method for atmospheric tomography”. In: *Proceedings of the Third AO4ELT Conference, S. Esposito and L. Fini, eds., Firenze*. 2013. DOI: 10.12839/AO4ELT3.13433.
- [60] M. Yudytskiy, T. Helin, and R. Ramlau. “Finite element-wavelet hybrid algorithm for atmospheric tomography”. In: *J. Opt. Soc. Am. A* 31 (2014), pp. 550–560.